nic rabbits ($2.1 \pm 0.5 \times 10^4$ μL^{-1}, $n = 7$), platelet counts gradually increased with time, reaching a maximum at 30 min after transfusion of $2.2 \pm 1.1 \times 10^4$, $4.0 \pm 1.1 \times 10^4$ and $6.1 \pm 0.8 \times 10^4$ μL^{-1}, respectively. At doses of 0.4×10^9, 2.0×10^9 and 4.0×10^9 kg^{-1}, dose-dependent reductions in bleeding time of 1505 ± 410, 867 ± 440 and 505 ± 257 s, respectively, were seen (Fig. 4B, $n = 7$). We also confirmed that bleeding time 30 min after PPP transfusion was 1473 ± 442 s (not shown, $n = 7$), almost comparable to that obtained with thrombocytopenic rabbits infused with saline (1695 ± 197 s, $n = 7$).

Recovery rates of H12-(ADP)-liposomes 30 min after infusion into normal rabbits was estimated to be $28 \pm 7\%$ ($n = 3$) and $T_{\beta 1/2}$ was 522 ± 30 min ($n = 3$) (not shown). Indeed, when H12-(ADP)-liposomes at doses of 10 and 20 mg kg^{-1} were infused into thrombocytopenic rabbits, a dose-dependent reduction in bleeding time was identified (Fig. 4B), with bleeding times significantly reduced to 881 ± 303 and 428 ± 44 s, respectively ($n = 6$). In contrast, bleeding times of (ADP)-liposome groups at doses of 10 and 20 mg kg^{-1} were 1429 ± 643 and 1375 ± 663 s, respectively ($n = 6$). These results strongly indicate that H12-(ADP)-liposomes exhibit *in vivo* hemostatic ability as efficient as platelet transfusion.

Changes in coagulation and platelet activation parameters after H12-(ADP)-liposome infusion

Blood coagulation parameters (PT, APTT and fibrinogen antigen levels) in thrombocytopenic rat and rabbit plasma at approximately 60 min after measurement of bleeding time were measured. No significant differences among groups were noted with saline, (ADP)- and H12-(ADP)-liposomes, suggesting that *in vivo* perturbation of coagulation pathway by these liposomes was unlikely (Table S2).

Next, we studied whether H12-(ADP)-liposomes infusion caused platelet activation in circulation (Table 1, Supporting information). When H12-(ADP)-liposomes were infused, platelets obtained at 10- to 60-min intervals showed minimal P-selectin expression that was just comparable to values obtained with saline infusion. Of note, infusion of 1 mmol L^{-1} of ADP solution also failed to activate circulating platelets. Furthermore, platelet counts were unchanged after infusion of H12-(ADP)-liposomes and ADP solution.

These results indicate that our H12-(ADP)-liposomes may be safe as a prototype platelet substitute that exerts platelet aggregation-augmenting effects at sites of bleeding but not in circulation.

Discussion

This communication reported a novel synthetic product composed of lipid nanovesicles (H12-(ADP)-liposomes) designed for targeting activated platelets at sites of vascular injury to help reinforce primary hemostasis by residual platelets in thrombocytopenia.

A notable observation was that H12-mediated interaction of liposome with activated platelets induces release of aqueous contents (CF dye) from the liposome in an aggregation-dependent manner (Fig. 2B). ADP is a weak agonist, but synergizes the effects of other aggregating agents even at suboptimal concentrations [13]. ADP also stabilizes aggregates formed by strong agonists such as thrombin [14]. In fact, by ADP encapsulation, H12-liposome could gain function to further augment platelet aggregation response triggered by a suboptimal concentration (0.4 μg mL^{-1}) of collagen (Fig. 1A). As the extent of aggregation response to low-dose collagen depends upon costimulation with agonists such as ADP released from secretary granules, aggregation response enhancement is probably attributable to ADP released from liposomes. The mechanism of aggregation-dependent ADP release from H12 liposome is currently unknown. A previous study with a different preparation of H12-coated liposomes showed that an encapsulated substance was released upon interaction with platelets activated on the collagen surface, and content release was dependent on ligand (H12) density and inhibited by either anti-H12 or anti-GPIIb/IIIa antibody [15]. The phenomenon can thus be postulated to possibly represent the result of liposome membrane perturbation or mixing rendered by physical force due to multivalent ligand-receptor coupling with activated platelets.

Our working hypothesis in developing an efficient platelet substitute was that H12-coated liposome is specifically and

Table 1 Flow cytometric analyses of P-selectin expression before and after infusion of H12-(ADP)-liposomes into rabbits

Time after infusion (min)	0	10	20	60
Platelet counts ($\times 10^5$ μL^{-1})				
Saline	3.3 ± 0.2	3.5 ± 0.5	3.4 ± 0.3	3.4 ± 0.2
H12-(ADP)-liposome	3.3 ± 0.4	3.2 ± 0.4	3.3 ± 0.5	3.4 ± 0.4
ADP solution (1 mmol L^{-1})	3.5 ± 0.2	3.5 ± 0.3	3.4 ± 0.2	3.4 ± 0.3
P-selectin expression (%)				
Saline	0.62 ± 0.10	0.59 ± 0.17	0.60 ± 0.07	0.58 ± 0.12
H12-(ADP)-liposome	0.56 ± 0.20	0.60 ± 0.19	0.58 ± 0.10	0.60 ± 0.16
ADP solution (1 mmol L^{-1})	0.55 ± 0.24	0.58 ± 0.07	0.56 ± 0.14	0.60 ± 0.10
Positive control	26.6 ± 8.2			

Positive controls showed P-selectin expression of platelet-rich plasma by stimulation with 5 μmol L^{-1} ADP. Data are the mean ± SD of three independent experiments.

effectively targeted at sites of injured vasculature where a hemostatic plug is being formed by remaining platelets in thrombocytopenia. The H12 sequence is thought to be a necessary and sufficient binding site of fibrinogen for the receptor to support optimal reactivity with platelets [16–19]. In addition, H12 peptides are known to have much higher receptor selectivity with GPIIb/IIIa as compared with that of RGD and fibrinogen, which are reactive with other integrins such as $\alpha_v\beta_3$, $\alpha_5\beta_1$ and $\alpha_M\beta_2$ expressed on blood cells including platelets and leukocytes, and vascular endothelium [8,20–22]. In fact, using CT analysis, we were able to demonstrate that, when injected intravenously into normal rats, H12-coated liposome containing iopamidol contrast dye was effectively and specifically concentrated at the site of injured vein along with skin incision of the tail (Fig. 3). Together with our series of *in vivo* observations including the present study (Fig. 4A) in which H12-coated albumin particles and liposomes displayed ability to reduce enhanced tail bleeding time in thrombocytopenic rats, the results suggest that the H12-coated product can exert hemostatic function at the vascular injury site, but not in circulation [9–11].

Our *in vivo* results clearly demonstrate the feasibility of H12-(ADP)-liposomes as a synthetic product to replace platelet transfusion for patients with thrombocytopenia. We showed that ADP encapsulation can effectively intensify the hemostatic ability of liposomes, suggesting that locally released ADP at vascular injury sites plays a significant role in primary hemostasis (Fig. 4A). A rabbit thrombocytopenia model then clearly showed that H12-(ADP)-liposomes exhibited a dose-dependent hemostatic effect as efficiently as that of fresh animal platelets (Fig. 4B). In practice, 4.0×10^9 cells kg^{-1} of platelet transfusion resulted in reduction of elongated ear bleeding time in thrombocytopenic rabbits from 1695 to 505 s, while platelet count could be corrected from 2.2×10^4 to 6.1×10^4 μL^{-1}. A nearly equivalent hemostatic effect (correction of bleeding time to 428 s) was obtained by 20 mg kg^{-1} (corresponding to 1.0×10^{13} particles kg^{-1}) of H12-(ADP)-liposome infusion. In the human setting, a standard dose of transfusion to yield clinical efficacy requires platelet concentrates containing at least 5.0×10^9 cells kg^{-1} [23]. Our rabbit model would thus simulate platelet transfusion in humans.

A major concern regarding the safety of this product involves whether enhanced platelet activation or thrombosis is induced in circulation. If ADP is recovered 100% from 20 mg kg^{-1} of H12-(ADP)-liposomes in rabbit plasma, the final ADP concentration is calculated as 5 $\mu mol\ L^{-1}$, a plasma level that would readily induce platelet activation and aggregation *in vitro* (Table 1). Local extracellular concentrations of ADP generated by maximal platelet aggregation are estimated to be around 20–30 $\mu mol\ L^{-1}$ in humans and rabbits [24]. However, the released ADP may be rapidly diluted by circulation or drastically hydrolyzed by nucleotidases present on the endothelium, leukocytes and in plasma to maintain nucleotide homeostasis [25,26]. In fact, no significant P-selectin expression (a sensitive platelet activation marker) on circulating platelets was detected in normal rabbits for 60 min after infusion of 20 mg kg^{-1} of liposome. In addition, even direct bolus infusion of extremely high concentrations of ADP (final plasma concentration, 100 $\mu mol\ L^{-1}$) did not induce P-selectin expression, suggesting that the plasma ADP catabolizing system *in vivo* is functional at least under conditions in which ADP concentrations temporarily reach the 100-$\mu mol\ L^{-1}$ range. Thus, together with the additional findings that liposome infusion had no effects on circulating platelet count (Table 1) and did not alter the plasma activity of coagulation parameters in rabbits (Table S2), our H12-(ADP)-liposomes may offer a suitable hemostatic agent that acts on activated platelets at sites of vascular injury, but not in circulation.

In conclusion, we have developed a synthetic platelet substitute comprising fibrinogen-derived H12 peptide-coated, ADP-encapsulated liposomes. As H12-(ADP)-liposomes exhibit *in vitro* function via activated platelets (Fig. 1), they seem to require endogenous platelets to work and thus may not be as effective if administered to patients with significant thrombocytopenia. At the same time, these liposomes may be useful to treat bleeding in patients with qualitative platelet disorders, such as storage pool deficiency. Further study is needed under conditions simulating various clinical settings to establish potential indications in platelet transfusion.

Acknowledgements

The authors wish to thank N. Watanabe, T. Kamata, K. Yokoyama and M. Murata at Keio University for valuable discussion and/or critical reading. This work was supported in part by Health and Labor Sciences Research Grants (Research on Public Essential Drugs and Medical Devices, S. Takeoka, Y. Ikeda and M. Handa) from the Ministry of Health, Labour and Welfare, Japan. Y. Okamura was the recipient of a research fellowship from the Japan Health Sciences Foundation.

Disclosure of Conflict of Interests

The authors state that they have no conflict of interest.

Supporting Information

Additional Supporting Information may be found in the online version of this article:

Table S1. PAC-1 binding to and P-selectin expression on platelets stirred with H12-(ADP)-liposome.

Table S2. Blood coagulation parameters in thrombocytopenic rats and rabbits after H12-(ADP)-liposome infusion.

Please note: Wiley-Blackwell are not responsible for the content or functionality of any supporting materials supplied by the authors. Any queries (other than missing material) should be directed to the corresponding author for the article.

References

1 Blajchman MA. Substitutes and alternatives to platelet transfusions in thrombocytopenic patients. *J Thromb Haemost* 2003; **1**: 1637–41.

2 Bode AP, Fischer TH. Lyophilized platelets: fifty years in the making. *Artif Cells Blood Substit Immobil Biotechnol* 2007; **35**: 125–33.
3 Agam G, Livine AA. Erythrocytes with covalently bound fibrinogen as a cellular replacement for the treatment of thrombocytopenia. *Eur J Clin Invest* 1992; **22**: 105–12.
4 Coller BS, Springer KT, Beer JH, Mohandas N, Scudder LE, Norton KJ, West SM. Thromboerythrocytes. In vitro studies of a potential autologous, semi-artificial alternative to platelet transfusion. *J Clin Invest* 1992; **89**: 546–55.
5 Andrieux A, Hudry-Clergeon G, Ryckewaert JJ, Chapel A, Ginsberg MH, Plow EF, Marguerie G. Amino acid sequences in fibrinogen mediating its interaction with its platelet receptor, GPIIbIIIa. *J Biol Chem* 1989; **264**: 9258–65.
6 Levi M, Friedrich PW, Middleton S, De Groot PG, Wu YP, Harris R, Biemond BJ, Heijjen FG, Levin J, Ten Cate JW. Fibrinogen-coated albumin microcapsules reduce bleeding in severely thrombocytopenic rabbits. *Nat Med* 1999; **5**: 107–11.
7 Takeoka S, Okamura Y, Teramura Y, Watanabe N, Suzuki H, Tsuchida E, Handa M, Ikeda Y. Function of fibrinogen γ-chain dodecapeptide-conjugated latex beads under flow. *Biochem Biophys Res Commun* 2003; **312**: 773–9.
8 Ruoslahti E. RGD and other recognition sequences for integrins. *Annu Rev Cell Dev Biol* 1996; **12**: 697–715.
9 Okamura Y, Takeoka S, Teramura Y, Maruyama H, Tsuchida E, Handa M, Ikeda Y. Hemostatic effects of fibrinogen γ-chain dodecapeptide-conjugated polymerized albumin particles in vitro and in vivo. *Transfusion* 2005; **45**: 1221–8.
10 Okamura Y, Fujie T, Maruyama H, Handa M, Ikeda Y, Takeoka S. Prolonged hemostatic ability of poly(ethylene glycol)-modified polymerized albumin particles carrying fibrinogen γ-chain dodecapeptide. *Transfusion* 2007; **47**: 1254–62.
11 Okamura Y, Maekawa I, Teramura Y, Maruyama H, Handa H, Ikeda Y, Takeoka S. Hemostatic effects of phospholipid vesicles carrying fibrinogen γ-chain dodecapeptide in vitro and in vivo. *Bioconjug Chem* 2005; **16**: 1589–96.
12 Okamura Y, Fujie T, Nogawa M, Maruyama H, Handa M, Ikeda Y, Takeoka S. Hemostatic effects of polymerized albumin particles carrying fibrinogen γ-chain dodecapeptide as platelet substitutes in severely thrombocytopenic rabbits. *Transfus Med* 2008; **18**: 158–66.
13 Ware JA, Smith M, Salzman EW. Synergism of platelet-aggregating agents. Role of elevation of cytoplasmic calcium. *J Clin Invest* 1987; **80**: 267–71.
14 Cattaneo M, Canciani MT, Lecchi A, Kinlough-Rathbone RL, Packham MA, Mannucci PM, Mustard JF. Released adenosine diphosphate stabilizes thrombin-induced human platelet aggregates. *Blood* 1990; **75**: 1081–6.
15 Nishiya T, Toma C. Interaction of platelets with liposomes containing dodecapeptide sequence from fibrinogen. *Thromb Haemost* 2004; **91**: 1158–67.
16 Kloczewiak M, Timmons S, Bednarek MA, Sakon M, Hawiger J. Platelet receptor recognition domain on the γ chain human fibrinogen and its synthetic peptide analogues. *Biochemistry* 1989; **28**: 2915–9.
17 Weisel JW, Nagaswami C, Vilaire G, Bennett JS. Examination of platelet membrane glycoprotein IIb-IIIa complex and its interaction with fibrinogen and other ligands by electron microscopy. *J Biol Chem* 1992; **267**: 16637–43.
18 Farrell DH, Thiagarajan P. Binding of recombinant fibrinogen mutants to platelets. *J Biol Chem* 1994; **269**: 226–31.
19 Holmbäck K, Danton MJ, Suh TT, Daugherty CC, Degen JL. Impaired platelet aggregation and sustained bleeding in mice lacking the fibrinogen motif bound by integrin αIIbβ3. *EMBO J* 1996; **15**: 5760–71.
20 Smith JW, Ruggeri ZM, Kunicki TJ, Cheresh DA. Interaction of integrins $\alpha_v\beta_3$ and GPIIb-IIIa with fibrinogen. *J Biol Chem* 1990; **265**: 12267–71.
21 Suehiro K, Gailit J, Plow EF. Fibrinogen is a ligand for integrin $\alpha_5\beta_1$ on endothelium cells. *J Biol Chem* 1997; **272**: 5360–6.
22 Yakubenko VP, Solovjov DA, Zhang L, Yee VC, Plow EF, Ugarova TP. Identification of the binding site for fibrinogen recognition peptide γ383-395 within the α_MI-domain of integrin $\alpha_M\beta_2$. *J Biol Chem* 2001; **276**: 13995–4003.
23 Norol F, Bierling P, Roudot-Thoraval F, Le Coeur FF, Rieux C, Lavaux A, Kuentz M, Duedari N. Platelet transfusion: a dose-response study. *Blood* 1998; **92**: 1448–53.
24 Meyers KM, Holmsen H, Seachord CL. Comparative study of platelet dense granule constituents. *Am J Physiol* 1982; **243**: R454–61.
25 Heptinstall S, Johnson A, Glenn JR, White AE. Adenine nucleotide metabolism in human blood – important roles for leukocytes and erythrocytes. *J Thromb Haemost* 2005; **3**: 2331–9.
26 Atkinson B, Dwyer K, Enjyoji K, Robson SC. Ecto-nucleotidases of the CD39/NTPDase family modulate platelet activation and thrombus formation: potential as therapeutic targets. *Blood Cells Mol Dis* 2006; **36**: 217–22.

Cystathionine β-Synthase as a Carbon Monoxide–Sensitive Regulator of Bile Excretion

Tsunehiro Shintani,* Takuya Iwabuchi,* Tomoyoshi Soga, Yuichiro Kato, Takehiro Yamamoto, Naoharu Takano, Takako Hishiki, Yuki Ueno, Satsuki Ikeda, Tadayuki Sakuragawa, Kazuo Ishikawa, Nobuhito Goda, Yuko Kitagawa, Mayumi Kajimura, Kenji Matsumoto, and Makoto Suematsu

Carbon monoxide (CO) is a stress-inducible gas generated by heme oxygenase (HO) eliciting adaptive responses against toxicants; however, mechanisms for its reception remain unknown. Serendipitous observation in metabolome analysis in CO-overproducing livers suggested roles of cystathionine β-synthase (CBS) that rate-limits transsulfuration pathway and H_2S generation, for the gas-responsive receptor. Studies using recombinant CBS indicated that CO binds to the prosthetic heme, stabilizing 6-coordinated CO-Fe(II)-histidine complex to block the activity, whereas nitric oxide (NO) forms 5-coordinated structure without inhibiting it. The CO-overproducing livers down-regulated H_2S to stimulate HCO_3^--dependent choleresis: these responses were attenuated by blocking HO or by donating H_2S. Livers of heterozygous CBS knockout mice neither down-regulated H_2S nor exhibited the choleresis while overproducing CO. In the mouse model of estradiol-induced cholestasis, CO overproduction by inducing HO-1 significantly improved the bile output through stimulating HCO_3^- excretion; such a choleretic response did not occur in the knockout mice. *Conclusion:* Results collected from metabolome analyses suggested that CBS serves as a CO-sensitive modulator of H_2S to support biliary excretion, shedding light on a putative role of the enzyme for stress-elicited adaptive response against bile-dependent detoxification processes. (HEPATOLOGY 2009;49:141-150.)

Carbon monoxide (CO) is generated from inducible heme oxygenase 1 (HO-1) and constitutive heme oxygenase 2 (HO-2), respectively, and has the ability to regulate neurovascular functions,[1,2] apoptotic responses,[3,4] and metabolism of xenobiotics and toxicants.[5,6] This gas is overproduced through increased delivery of heme as a substrate and the HO-1 induction on exposure to stressors such as hypoxia and oxidative stress. Mechanisms by which CO regulates cell functions appear to involve an activation of soluble guanylate cyclase (sGC), the enzyme that allows the gas to bind to the prosthetic heme to synthesize cyclic guanosine monophosphate as a second messenger.[1] Distinct from nitric oxide (NO) that forms 5-coordinated NO-Fe(II) complex to trigger full activation of the enzyme, CO activates this enzyme only modestly because the gas binding stabilizes 6-coordinated CO-Fe(II)-histidine complex.[7] Mitogen-activated protein kinase has also been shown to serve as a CO-responsive signal transducer.[8] Gene disruption of HO-1 increases sensitivity to overproduction of reactive oxygen species, inflammatory mediators or xenobiotic metabolism, whereas the gene transfer or CO inhalation under these circumstances suppresses such pathogenic responses.[7-9] However, direct mechanisms for the CO reception to trigger these adaptive responses of metabolism remain unknown.

Because this gas has the ability to inhibit ferrous form of the prosthetic heme of enzymes, tryptophan 2,3-dioxygenase or cytochromes P450 have been considered puta-

Abbreviations: CBS, cystathionine β-synthase; CE-MS, capillary electrophoresis equipped with mass spectrometry; CO, carbon monoxide; CORM, CO-releasing metal carbonyl tricarbonyldichlororuthenium (II); ES, 17α-ethinylestradiol; GSH, glutathione; GSNO, S-nitrosyl glutathione; H12, liver exposed to 12-hour hemin treatment; NO, nitric oxide; $RuCl_3$, CO-free ruthenium (III) chloride; SAM, S-adenosyl methionine; SE, standard error; sGC, soluble guanylate cyclase.

From the Department of Biochemistry and Integrative Medical Biology, Department of Surgery, School of Medicine, Keio University, Tokyo, Japan; the Institute for Advanced Biosciences, Keio University, Tsuruoka City, Japan; and the First Department of Surgery, College of Medicine, Nagoya University, Nagoya, Japan.

Received July 3, 2008; accepted August 25, 2008.

**These authors contributed equally to this work.*

T.H. is a postdoctoral research fellow supported by Grant-in-Aid for Creative Scientific Research 17GS0419 from JSPS in Japan. Development of the methodology for differential metabolomic analyses using contrast-enhanced time of flight/mass spectrometry was supported by Leading Project for Biostimulation from MEXT. T.I. and T.Y. are research associates of Global COE Program for Metabolomic Systems Biology from MEXT and MHLW.

Address reprint requests to: Makoto Suematsu, M.D., Ph.D., Professor and Chair, Department of Biochemistry and Integrative Medical Biology, School of Medicine, Keio University, 35 Shinanomachi, Shinjuku-ku, Tokyo 160-8582, Japan. E-mail: msuem@sc.itc.keio.ac.jp; fax: (81)-3-5363-3466.

Published online in Wiley InterScience (www.interscience.wiley.com).

DOI 10.1002/hep.22604

Potential conflict of interest: Nothing to report.

tive CO-sensitive signal transducers regulating cell functions, including cell proliferation,[10] immune responses,[11] microvascular tone, xenobiotic detoxification, and biliary excretion in the liver.[5,6,12] However, ferrous heme of these enzymes is not only sensitive to CO but to NO. In this context, whether mechanisms by which CO regulates cell and organ functions is not shared by those for NO has not fully been studied yet.

This study aimed to mine novel CO-responsive regulators for stress-inducible adaptation of metabolism. To this end, we have used metabolome analyses based on capillary electrophoresis equipped with mass spectrometry (CE-MS) for systematic mining CO-responsive gaseous signal transducers. The current results suggest that cystathionine β-synthase (CBS), the enzyme rate-limiting transsulfuration pathway is such a novel CO-sensitive regulator of metabolism that plays an important role for quality control of bile excretion under disease conditions.

Materials and Methods

Preparation of Mice. The experimental protocols herein described were approved by our institutional guidelines provided by the Animal Care Committee of Keio University School of Medicine. Mice heterozygous for disruption in the CBS gene were purchased from Jackson Labs (Bar Harbor, MI) and bred at our institution. Male heterozygous CBS-deficient mice ($CBS^{+/-}$) and their littermates ($CBS^{+/+}$), and wild-type B6J mice, which were purchased from Clea Japan, Inc (Kawasaki City, Japan), were used at 8 to 12 weeks of age. Mice were allowed free access to laboratory chow and tap water, and were fasted for 18 hours before experiments. Mice were anesthetized with an intraperitoneal injection of ketamine at 120 mg/kg, and xylidine at 6 mg/kg. Their common bile ducts were ligated in proximity to the duodenum, and the gallbladder was nicked and cannulated with a polyethylene P-10 tube to collect bile for 20 minutes after a 10-minute stabilization period.[6,13] Biliary constituents such as total bile salts, bilirubin-IXα, pH values, and bicarbonate (HCO_3^-) were measured according to previous methods described elsewhere.[13] When necessary, biliary samples were collected into tubes containing 10% trichloroacetate to measure glutathione through high-performance liquid chromatography.[14] Determination of bilirubin-IXα in bile serves as an indicator of HO-mediated heme degradation in the liver that occurs in parallel with endogenous CO generation. Hepatic CO contents were also measured by gas chromatography as described previously,[15] except that the flame ionization detector equipped with a methanizer was used in this study instead of a reduction gas detector. Combination of these methods to determine CO allowed us to distinguish endogenous CO generation from the same gas exogenously administered as an intervention as described in the following session.

Administration of Reagents Studied. Protoheme IX (hemin) was administered at 40 μmol/kg intraperitoneally at 12 hours before surgical preparation for bile collection. This protocol was denoted as liver exposed to 12-hour hemin treatment (H12) treatment in the text. After collecting bile, livers were excised immediately to be snap-frozen in cold methanol, and the lysates served as samples for contrast-enhanced time of flight/mass spectrometry analyses as described later. In separate sets of experiments, liver samples were minced with 10% trichloroacetic acid at 4°C to measure cysteine and glutathione (GSH) through high-performance liquid chromatography to confirm the data collected from contrast-enhanced time of flight/mass spectrometry, when necessary.

A series of protocols were employed to examine roles of HO-derived CO in regulation of H_2S-modulated choleresis in the H12-treated mice. First, zinc protoporphyrin, a potent HO inhibitor, was administered intravenously at 12.5 μmol/hour/kg at 30 minutes before the bile collection; this dose was sufficient to block endogenous CO in the liver. When necessary, tricarbonyldichlororuthenium (II) dimer, the CO-releasing metal carbonyl [tricarbonyldichlororuthenium (II): CORM, Sigma-Aldorich][16] was administered intraportally at 30 minutes before the start of bile collection. When necessary, CO-free ruthenium (III) chloride ($RuCl_3$) was used as a negative control reagent. To examine whether the elevation of H_2S in the liver could alter biliary HCO_3^- excretion, sodium hydrosulfide (NaHS) was administered at 20 μmol/hour/kg through the portal vein at 30 minutes before the bile collection; as seen later in Results, this protocol restored the H12-induced decrease in the hepatic H_2S contents without altering a reduction of systemic blood pressure that was induced by a systemic bolus of the NaHS injection. S-nitrosyl glutathione (GSNO) was used as an NO donor. The reagent was injected intraportally with a dose of 7 μmol/kg at 30 minutes before the collection of bile; this protocol did not induce a reduction of systemic blood pressure, whereas greater doses caused hypotension and subsequent decrease in the bile output. In these experiments, administration of the reagent was performed through a 30-gauge miniature needle that was inserted into the portal vein to be fixed at the site of puncture. Finally, to examine therapeutic effects of CO, we examined effects of H12 treatment or administration of CORM in the mice exposed to drug-induced cholestasis. To this end, cholestasis was induced by a subcutane-

ous injection of 17α-ethinylestradiol (ES) at 5 mg/kg daily for 5 consecutive days before the experiments.[17]

Metabolome Analysis. We performed metabolome analyses of tissue lysates collected from snap-frozen livers of mice using contrast-enhanced time of flight/mass spectrometry according to our previous methods.[18,19] Measurements of hepatic H_2S contents were based on gas chromatography described in our previous method.[14] Biliary flux of bilirubin-IXα (BR-IXα) in bile samples were determined by enzyme-linked immunosorbent assay using the anti–BR-IXα monoclonal antibody as described previously.[6,20] Because BR-IXα is an end product of the HO-mediated degradation of protoheme IX, its measurements in bile serves as an index of endogenous CO generation in the liver.[20] The conversion of ^{15}N-methionine to its downstream metabolites was determined by CE-MS to examine different rates of the metabolic flux through CBS in the liver. In these experiments, ^{15}N-methionine was intraperitoneally injected at 150 μmol/100 g body weight, and ^{15}N-homocysteine and ^{15}N-cystathionine were measured by CE-MS using the lysates of liver tissues at 30, 60, and 120 minutes after the methionine challenge. Data were expressed as percentages of the mass-labeled metabolites versus total amounts of metabolites in remethylation cycle [ΣRM: methionine + S-adenosyl methionine (SAM) + S-adenosyl homocysteine (SAH) + homocysteine]. In a separate set of experiments, effects of application of CO on contents of methionine and cystathionine in HepG2 cells were determined in culture. In these experiments, the cells were maintained in Roswell Park Memorial Institute 1640 medium (Invitrogen, Carlsbad, CA) containing 10% fetal bovine serum; the mixture was supplemented with 1× penicillin/streptomycin and maintained at 37°C in an atmosphere of 5% CO_2/95% air. The cells were treated with either 50 μmol/L CORM or $RuCl_3$ as a negative control for 16 hours. To measure the metabolites, a frozen pellet of the 1×10^6 cells was homogenized in 10% trichloroacetic acid with 10 mM diethylene triamine pentaacetic acid following brief centrifugation, and the supernatant was used as a sample.

Western Blot Analysis. Western blot analysis was carried out to examine an induction of heme oxygenase (HO)-1 using the polyclonal antibody SPA896 (Stressgen, Ann Arbor, MI). In these experiments, the blotting against α-tubulin was carried out using the polyclonal antibody (Cell Signaling, Danvers, MA) as an internal control.

Recombinant Full-Length Rat CBS. The complementary DNA of the full-length rat CBS was a gift from Professor Masao Ikeda-Saito in Tohoku University. Stopped-flow equipment was purchased from Unisoku, Inc. (Tokyo) and used to examine binding of CO or NO to the CBS protein according to previous methods.[21] Electron paramagnetic resonance spectrometry to determine 5-coordinated structure of the nitrosylheme complex of CBS was carried out according to previous methods.[21,22]

Statistical Analyses. The statistical significance of data among different experimental groups was determined by one-way analysis of variance and Fischer's multiple comparison test. $P < 0.05$ was considered significant.

Results

CO Overproduction Inhibits Transsulfuration and H_2S and Stimulates HCO_3^- Choleresis. Metabolome analyses based on CE-MS allowed us to pinpoint metabolic pathways responding to disease conditions. In mouse liver, we detected more than 1800 metabolites, and compared differences between the control and acetaminophen-treated livers.[18] This method was used to determine differences in metabolic responses between mouse livers and those overloaded with heme, the stressor inducing oxidative stress and subsequent CO overproduction through increasing the substrate and inducing HO-1 (Fig. 1A). The hepatic CO flux peaked at 6 hours, becoming threefold to fourfold greater during the 6 to 12 hours after challenging with hemin, as judged by BR-IXα, an end product of HO-mediated heme degradation (Fig. 1B).[13] Under these conditions, bile output was modestly but significantly increased at 12 to 18 hours after the treatment (Fig. 1C) in parallel with significant elevation of HCO_3^- to make bile more alkaline (Fig. 1D-F), enhancing solubility of organic anions during the detoxification processes. These results suggest that the heme-elicited choleretic response is not correlated with vasodilatory mechanisms by the gas. Based on these results, we used CE-MS analyses to examine metabolomics in the liver exposed to 12-hour hemin treatment (H12), in which phenotypes of bile remodeling became evident.

Among known metabolites (Table 1), most prominent differences between the control and H12 groups occurred in global decreases in amino acids concurrent with increases in Krebs cycle substrates such as acetyl CoA: the fact that these changes coincided with sustained glutamate, significant increases in glutamine, and high-energy adenosine phosphates appeared to suggest utilization of the amino acid pool for energy substrates. By contrast, several essential amino acids such as methionine, tryptophan and histidine, and serine were maintained. Another important alteration was a global decrease in transsulfuration metabolites such as cystathionine, cysteine, and

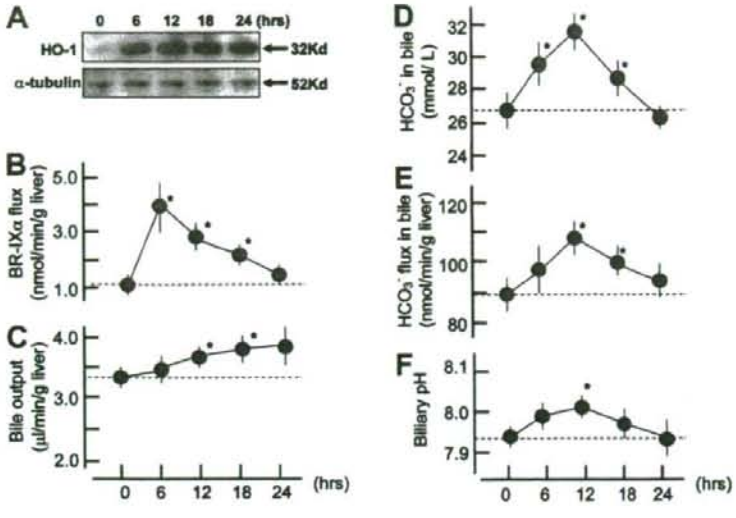

Fig. 1. Temporal alterations in hepatic generation of CO and biliary function after overloading heme. (A) Western blots indicating the induction of heme oxygenase (HO)-1. Alpha-tubulin is an internal control. (B) Biliary excretion of bilirubin-IXα (BR-IXα), a terminal metabolite of HO-dependent heme degradation, as an index of endogenous CO generation through heme oxygenase in the liver. (C) Bile output. (D) Biliary concentration of HCO_3^-. (E) Biliary flux of HCO_3^-. (F) pH values of bile. $^*P < 0.05$ versus the value measured at time 0, which is before the intraperitoneal hemin administration at 40 μmol/kg.

hypotaurine. These results led us to determine tissue contents of H_2S, the terminal product derived from CBS or cystathionine γ-lyase that constitute transsulfuration pathway; this gaseous compound turned out to be suppressed in the H12 group. Based on these measurements, we hypothesized that the H12 treatment limits the activity of CBS so far as judged from maintenance of methionine pool (ΣRM) and serine, a substrate of the enzyme, with suppression of the transsulfuration metabolites residing in the downstream (Fig. 2A). This hypothesis was confirmed by in vivo pulse-chase analysis showing accumulation of ^{15}N-homocysteine and suppression of ^{15}N-cystathionine after the ^{15}N-methionine challenge in the H12 group (Fig. 2B).

Such an inhibitory action of the H12 treatment on the transsulfuration pathway was reproducible when HepG2 cells was treated with CO in culture; contents of cystathionine were significantly suppressed by the application of 50 μmol/L CORM (9.3 ± 1.3 versus 15.9 ± 1.4 nmol/g protein for the vehicle treatment with $RuCl_3$. Mean ± standard error (SE) of three separate experiments, $P < 0.03$), whereas methionine exhibited no difference (66.3 ± 3.7 versus 80.3 ± 12.2 nmol/g protein for CORM and $RuCl_3$, respectively. Mean ± SE of three separate experiments), suggesting inhibitory action of the gas on CBS.

CO But Not NO Inhibits CBS. H12-induced metabolomic changes indicating dissociation between remethylation cycle and transsulfuration pathway led us to hypothesize that CBS, a heme-containing enzyme that rate-limits the transsulfuration pathway, is a sensor of the H12-elicited CO overproduction. Rat full-length recombinant CBS were purified (Fig. 3A) to examine whether CO or NO could inhibit the enzyme activities. CO, but not NO, specifically inhibited the enzyme (Fig. 3B). Previous crystallographic studies using a truncated form of CBS showed that the axial ligands for the prosthetic heme were cysteine and histidine, indicating a large peak of absorbance at 448 nm.[23] On CO application, the heme formed a 6-coordinated CO-Fe(II)–histidine complex, as judged by a decrease in the absorbance at 448 nm and a reciprocal elevation at 422 nm (Fig. 3C). These results were consistent with previous works using the truncated form of human recombinant CBS.[24] Such an inhibitory effect of CO on CBS activity occurred even when sufficient amounts of SAM were present as an allosteric activator,[25] whereas the CO concentrations necessary to suppress CBS became greater in the presence of SAM (Fig. 3D). Conversely, NO was able to bind to the heme but with a distinct structure of 5-coordinated nitrosyl-heme as judged by electron paramagnetic resonance spectrometry (Fig. 3E), suggesting that the enzyme responds specifically to the binding of CO but not that of NO.

CO-Induced HCO_3^- Choleresis Is Sensitive to H_2S and Disappears in $CBS^{+/-}$ Mice. Recent studies indicated that H_2S derived from cystathionine γ-lyase, an enzyme using cysteine to generate the gas, modulates biliary HCO_3^- excretion via mechanisms involving glibenclamide-sensitive channels, a putative H_2S target.[14,26] We hypothesized that the stress-induced CO stimulates the HCO_3^- excretion to increase pH in bile through its inhibitory action on CBS-derived H_2S. To examine this hypothesis, we chose the dose of the CO-releasing molecule (CORM) that was able to increase hepatic contents

Table 1. Comparison of Metabolome Analysis by CE-MS in Liver Extracts Between Control and the Hemin-Treated (H12) Mice

	Control	H12
Carbohydrates (nmol/g liver)		
Glucose 1-P	20 ± 4	31 ± 5
Glucose 6-P	24 ± 1	22 ± 6
Ribulose 5-P	206 ± 60	115 ± 17
Fructose 6-P	25 ± 1	21 ± 6
Glycerol 3-P	1800 ± 250	1663 ± 218
Lactate	3490 ± 633	2920 ± 385
Acetyl CoA	3.4 ± 0.5	6.2 ± 1.1*
Malonyl CoA	37 ± 6	83 ± 15*
Citrate	70 ± 13	88 ± 20
Fumarate	120 ± 22	167 ± 52
Malate	343 ± 91	479 ± 90
CoA	132 ± 21	111 ± 20
Nucleotides (nmol/g liver)		
ATP	208 ± 35	480 ± 90*
GTP	33 ± 4	79 ± 14*
ADP	577 ± 104	1060 ± 154*
AMP	1866 ± 277	1863 ± 70
IMP	501 ± 82	660 ± 99
Adenosine	203 ± 18	151 ± 11
Adenine	12 ± 1	12 ± 2
Hypoxanthine	58 ± 8	43 ± 15
	Control	**H12**
Amino acids (μmol/g liver)		
Gly	3.16 ± 0.11	2.20 ± 0.05*
Ala	3.12 ± 0.48	1.47 ± 0.40*
Ser	0.38 ± 0.07	0.31 ± 0.05
Pro	0.37 ± 0.03	0.27 ± 0.04*
Val	0.41 ± 0.01	0.23 ± 0.05*
Thr	0.31 ± 0.03	0.20 ± 0.04*
Lys	0.69 ± 0.13	0.46 ± 0.05*
Cys	0.20 ± 0.04	0.07 ± 0.03*
Leu	0.36 ± 0.02	0.25 ± 0.05†
Asp	0.76 ± 0.13	0.59 ± 0.12†
Glu	2.90 ± 0.16	2.75 ± 0.28
Gln	3.39 ± 0.58	6.48 ± 0.54*
His	0.43 ± 0.05	0.48 ± 0.02
Amino acids and derivatives (nmol/g liver)		
Met	49 ± 5	39 ± 10
GABA	29 ± 2	25 ± 4
Ornithine	420 ± 95	226 ± 22*
Asn	77 ± 7	59 ± 3*
Ile	175 ± 12	94 ± 17*
Arg	8.8 ± 1.2	4.8 ± 0.6*
Citrulline	64 ± 10	35 ± 3*
Trp	34 ± 2	31 ± 3
Tyr	111 ± 15	52 ± 8*
Glu-2 aminobutyrate	6.3 ± 2.3	5.7 ± 1.2
Ophthalmate	67 ± 7	83 ± 6

Data indicate mean ± SE of six separate experiments.

Data of metabolites in remethylation cycle and transsulfuration pathway were indicated in Fig. 2A.

*$P < 0.05$ and †$P < 0.1$ versus controls.

of CO comparably to those measured in the H12 treatment: As seen (Fig. 4A), the intraportal administration of CORM at 20 μmol/kg significantly increased hepatic CO contents comparable to those induced by H12 treatment in the intact mice. This dose of CORM suppressed hepatic H_2S and stimulated biliary HCO_3^- flux. Stimulatory effects of CO administration on biliary HCO_3^- excretion in intact mice were not shared by NO, as judged by observation in the mice administered with GSNO, an NO donor (Fig. 4B): These results were consistent with observation that CBS is sensitive to CO but not to NO in vitro (Fig. 3).

As already seen, H12 treatment increased CO generation (biliary BR-IXα flux), decreased hepatic H_2S contents, and stimulated biliary HCO_3^- flux (Fig. 1). HO blockade by zinc protoporphyrin-IX cancelled these changes elicited by H12 treatment. On the other hand, an administration of NaHS, an H_2S donor, abolished the H12-induced suppression of hepatic H_2S contents, and significantly attenuated the stimulatory response of biliary HCO_3^- flux (Fig. 5A), suggesting that H12-inducible CO stimulates biliary HCO_3^- excretion through modulation of CBS-derived H_2S. As previously reported, homozygous CBS knockout mice died of severe hepatic steatosis, whereas heterozygous knockout ($CBS^{+/-}$) mice survive through compensation without apparent phenotypes.[27] In these mice, indeed, the baseline H_2S content in livers of $CBS^{+/-}$ mice was comparable to that of $CBS^{+/+}$ mice, presumably because of compensation of the gas generation through cystathionine γ-lyase. On H12 treatment, $CBS^{+/-}$ mice exhibited an increase in the hepatic CO generation comparably to $CBS^{+/+}$ mice, but neither decreased H_2S contents nor up-regulated biliary HCO_3^- flux (Fig. 5B), indicating phenotypes distinct from those in $CBS^{+/+}$ littermates.

CO Protects Against Drug-Induced Cholestasis Through Mechanisms Involving CBS. We further attempted to investigate whether the administration of CO could improve biliary dysfunction occurring in disease models. To examine this, the mice were treated with ES, a cholestatic reagent suppressing three major osmolites such as HCO_3^-, glutathione, and bile salts in bile.[17] H12 treatment or the administration of CORM significantly increased bile output concurrently with a recovery of HCO_3^- excretion into bile (Fig. 6A). The anti-cholestatic effects of H12 treatment through stimulation of HCO_3^- excretion disappeared in the $CBS^{+/-}$ mice (Fig. 6B), suggesting again a pivotal role of CBS for triggering the CO-induced choleresis.

Discussion

CO administration or HO-1 induction has been shown to protect against tissue injury and considered a potentially useful therapeutic stratagem.[8,16] Serendipitous observation in the liver indicating effects of overproduced CO on metabolism of sulfur-containing amino

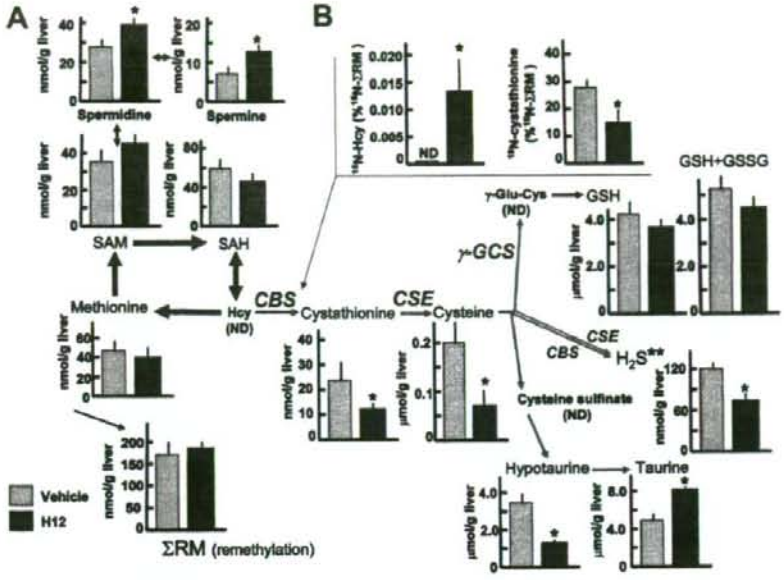

Fig. 2. Metabolomic comparison of sulfur-containing amino acids and their derivatives between the heme-overloaded and vehicle-treated livers of mice. (A) Differences in hepatic contents of the metabolites between the control and hemin-treated mice. H12: treatment with hemin at 12 hours before sampling the liver. Note decreases in transsulfuration metabolites. (B) *In vivo* pulse-chase analysis indicating conversion rates of ^{15}N-methionine into ^{15}N-homocysteine (Hcy) and ^{15}N-cystathionine in livers between the groups. The amounts of the downstream metabolites were measured at 30 minutes after the methionine administration. The data in B were normalized by total amounts of metabolites in remethylation cycle (^{15}N-methionine + ^{15}N-SAM + ^{15}N-SAH + ^{15}N-Hcy = ΣRM) at 30 minutes. ND, not detected. Data indicate mean ± SE of six to eight separate experiments for each group. $*P < 0.05$ versus the vehicle-treated group.

acids led us to reveal unique physiological actions of this gas on CBS *in vivo* that are not shared with NO. The current study suggested that stress-inducible CO targets CBS and thereby reduces H_2S significantly to stimulate biliary HCO_3^- excretion that could benefit detoxification processes. Conversely, such a property of stress-inducible CO might jeopardize anti-oxidative defense systems through an overflow of homocysteine or through a shortage of GSH. Under current experimental conditions, however, such a risk seemed little, if any, so far as judged from maintenance of GSH and adenosine triphosphate so far. This appears to result from large difference in amino acid pools between methionine (nmol/g) and thiols including cysteine and GSH (μmol/g). Furthermore, cysteine could be supplied through its uptake from extracellular space by mechanisms involving Nrf2, the transcriptional factor activated in response to oxidative stress or electrophiles such as heme.[28,29] By contrast, the amounts of sulfur-containing amino acids consumed to generate H_2S seems relatively smaller than that for synthesizing GSH or hypotaurine, as judged from quantitative information collected by metabolome analysis. Because CBS not only limits synthesis of cystathionine from homocysteine but also directly suppresses H_2S generation from cysteine, the inhibitory effects of CO on the enzyme could dictate largely on the action of H_2S in the liver, causing a stimulatory effect on bile excretion. Considering recent studies suggesting vasodilatory effects of H_2S,[26,30] suppression of CBS-derived H_2S by stress-inducible CO might trigger vasoconstriction, but such vasoactive responses did not occur so far as judged from choleretic response of the basal bile flow that is highly dictated by microvascular perfusion. This might result from the fact that stress-inducible CO itself has the ability to maintain the basal microvascular perfusion through multiple vasodilatory mechanisms involving activation of cyclic guanosine monophosphate and modulation of cytochrome P450–derived vasoconstrictors.[6,20,31]

Although the inhibitory action of stress-inducible CO on the transsulfuration pathway has first been shown in the heme-overloading detoxification model of mice in the current study, a similar event occurred in acetaminophen-induced acute liver injury model of mice in which CO was overproduced through degradation of cytochrome P450–derived heme.[5,18] Our previous study in rats suggested that another HO-derived product bilirubin but not CO

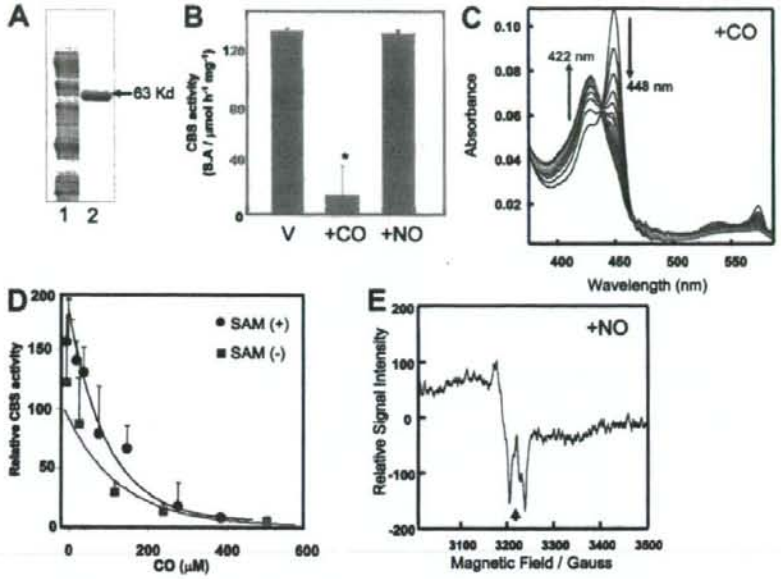

Fig. 3. Effects of CO and NO on the activity and structure of the prosthetic heme of rat recombinant full-length CBS. (A) Sodium dodecyl sulfate polyacrylamide gel electrophoresis for purification of rat recombinant CBS. Lane 1, crude extract; lane 2, purified CBS. (B) Effects of CO and NO on the Fe(II)-CBS activity under optimal substrate conditions at pH 7.4. CO but not NO (100 μM) significantly attenuated the activities of the ferrous enzyme. Data indicate mean $\pm$ SE of four experiments. The activities were measured by determining conversion of homocysteine and serine to cystathionine. $^*P < 0.05$ versus the group treated with vehicle (V). The concentration of CBS-heme was 10 μM. (C) Stopped-flow visible spectrophotometry for Fe(II)-CBS to examine temporal transitional changes after mixing with CO. Data exhibited a drop at 449 nm and a reciprocal elevation at 422 nm, demonstrating stabilization of the 6-coordinated CO-Fe(II)-histidine complex. $K_{obs} = 0.638$/second. (D) Effects of CO on the CBS activities in the presence or absence of S-adenosyl methionine (SAM), the allosteric activator of the enzyme. (E) Electron spin resonance spectrometry indicating 5-coordinated NO-Fe(II) complex of the CBS-heme. Arrow: g-value = 2.008.

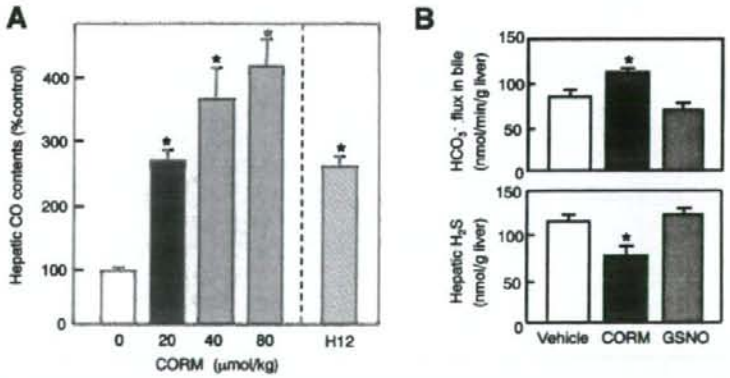

Fig. 4. Effects of the administration of CORM on hepatic CO delivery and biliary function, and their comparison with GSNO, an NO donor. (A) Effects of administration of CORM on hepatic CO contents. H12: the CO contents measured at 12 hours after an intraperitoneal injection of hemin at 40 μmol/kg. Data indicate mean $\pm$ SE of five separate experiments for each group. $^*P < 0.05$ versus the controls. Note that 20 μmol/kg CORM caused an increase comparable to that induced by H12. (B) Effects of an intraportal administration of CORM on hepatic H_2S contents and biliary HCO_3^- flux. GSNO, S-nitrosyl glutathione, an NO donor. $^*P < 0.05$ versus the values in the vehicle-treated controls. Data indicate mean $\pm$ SE of seven to eight separate experiments for each group.

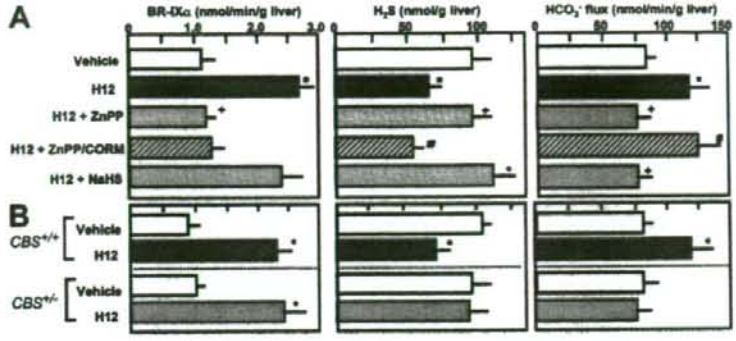

Fig. 5. Effects of HO blockade by zinc protoporphyrin and supplementation of NaHS, an H_2S donor, on biliary flux of BR-IXα, hepatic H_2S contents, and biliary HCO_3^- excretion in the 12-hour hemin-treated liver (H12). (A) Measurements in wild-type male B6 mice. Note that the hemin-induced suppression of H_2S generation and stimulation of biliary HCO_3^- excretion were sensitive to the HO inhibitor and reversed by supplementing CO (CORM). An injection of NaHS, an H_2S donor, restored hepatic H_2S contents and repressed the biliary HCO_3^- excretion in the H12-treated liver, suggesting that the biliary response is H_2S-dependent. (B) Disappearance of H12-induced reduction of H_2S and biliary HCO_3^- excretion in heterozygous CBS-knockout mice ($CBS^{+/-}$). Note that $CBS^{+/-}$ mice neither exhibit a reduction of H_2S nor up-regulate biliary HCO_3^- excretion, although overproducing CO (BR-IXα flux) comparably to the littermates ($CBS^{+/+}$). *$P < 0.05$ versus the vehicle-treated controls. +$P < 0.05$ versus the H12-treated groups. #$P < 0.05$ versus the H12+ zinc protoporphyrin-treated groups.

has the ability to improve bile acid–dependent bile output of the post–cold ischemic liver grafts through its antioxidative action.[32] However, such an effect of bilirubin appears to be distinct from the stimulatory action of CO on biliary fluid excretion indicated in the current study. CO has been shown to exert diverse actions on biliary function through multiple mechanisms: First, stress-inducible levels of CO have the ability to elongate the intervals of bile canalicular contraction, which helps increase the stroke volume for promoting bile excretion; this process appears to involve mechanisms mediated by modulation of cytochrome P450 epoxygenases and intra-

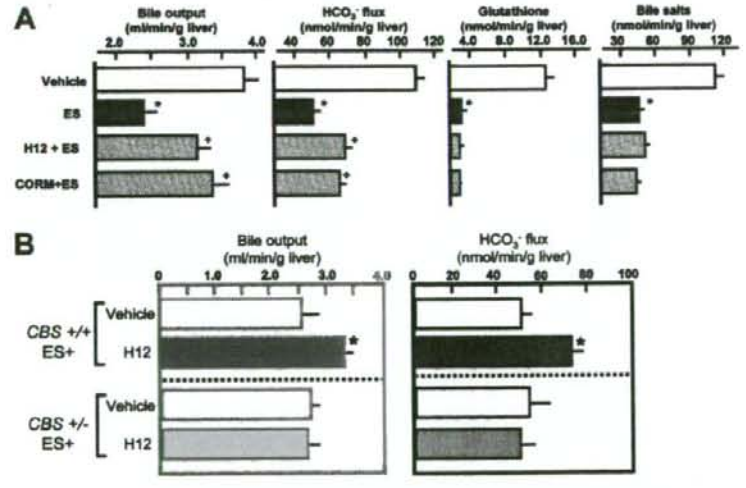

Fig. 6. Effects of H12 treatment or CORM administration on 17α-ethinylestradiol (ES)-induced cholestasis in male B6 mice. (A) Effects of H12 or CORM on ES-induced decreases in the bile output and bile constituents. ES elicited marked cholestasis, which coincided with decreases in HCO_3^-, glutathione, and bile salts in bile. Pretreatment with hemin at 12 hours before the administration of ES (H12 + ES) or the administration of CORM significantly attenuated ES-induced cholestasis through stimulation of HCO_3^- excretion into bile. (B) Effects of H12 treatment on ES-induced impairment of bile output and biliary HCO_3^- flux in $CBS^{+/+}$ and $CBS^{+/-}$ mice. *$P < 0.05$ versus the values in vehicle-treated controls. +$P < 0.05$ versus the values in ES-treated group. Data indicate mean ± SE of eight separate experiments for each group. Note disappearance of the improving effect of H12 treatment in the $CBS^{+/-}$ mice.

cellular Ca^{2+} mobilization.[12] Second, suppression of endogenous CO activates bile acid–dependent bile excretion through accelerated vesicular transport of taurocholate, while inducing no significant elevation of the bile acid–independent fraction.[33] Conversely, CO overproduction by the HO-1 induction or exogenous administration of CO stimulates bile acid–independent choleresis concurrently with increased mrp2-dependent excretion of bilirubin-IXα and glutathione, while suppressing biliary excretion of bile salts, indicating the effects of the gas for stimulating fluid excretion into bile.[34] Of interest is that glibenclamide, an inhibitor of K^+ channel that serves as a putative target for H_2S,[26] acts on Na^+-K^+-$2Cl^-$ cotransporter in bile duct epithelium to stimulate biliary HCO_3^- excretion in normal and cholestatic livers.[35] We showed that inhibition of cystathionine γ-lyase, another H_2S-generating enzyme, stimulates basal and glibenclamide-induced fluid output of bile through stimulating HCO_3^- excretion without altering the baseline vascular resistance of the liver.[14] Recent studies provided evidence that such a glibenclamide-responsive channel is present in rodent cholangiocytes[36] or in duodenum,[37] contributing to stimulation of the HCO_3^- excretion.[36] Based on these observations, it is not unreasonable to speculate that CO stimulates biliary fluid excretion through mechanisms involving H_2S-mediated modulation of glibenclamide-sensitive channels on biliary epithelium. Although further investigation is necessary to determine whether these mechanisms are sensitive to H_2S, the current results shed light on a possibility that the CO-CBS system serves as a putative mechanism for stimulating bile acid–independent fluid excretion, facilitating excretion of HCO_3^- and organic anions such as bilirubin to support heme detoxification. Both glibenclamide and CO help biliary fluid excretion in estrogen-induced hepatocellular cholestasis. Exploration of H_2S-sensitive molecular targets occurring on biliary epithelium deserves further studies for evidence that HO-1–derived CO serves as a therapeutic stratagem for protecting against cholestasis.

CO has been believed to share varied physiological effects on biological systems with NO. However, through extrapolation of studies *in vitro* indicating biochemical actions of CO to trigger structural changes in gas-responsive heme proteins (such as sGC, hemoglobin) distinct from those elicited by NO,[7,19,21,22,38] evidence that CO is a unique gaseous regulator distinct from NO has been emerging. In fact, CO itself modestly activates sGC, by which hepatic sinusoids are constitutively dilated.[2,20,39] By contrast, in vascular smooth muscle cells in which NO is sufficiently supplied from arteriolar endothelium (for example, brain microcirculation), the inducible CO inhibits NO-elicited sGC activation.[40,41] Besides these observations suggesting physiologic actions of CO occurring dependently of local NO levels, the current study provided evidence for a novel mechanism functioning irrespective of the NO effects. Furthermore, our results shed light on a metabolic link between CO and H_2S, suggesting that different gaseous mediators constitute an intriguing link for regulation of organ functions.

Acknowledgment: The authors thank Kayo Maruyama for technical support in measuring tissue H_2S contents.

References

1. Verma A, Hirsch DJ, Glatt CE, Ronnett GV, Snyder SH. Carbon monoxide: a putative neural messenger. Science 1993;259:381-384.
2. Suematsu M, Goda N, Sano T, Kashiwagi S, Egawa T, Shinoda Y, et al. Carbon monoxide: an endogenous modulator of sinusoidal tone in the perfused rat liver. J Clin Invest 1995;96:2431-2437.
3. Ozawa N, Goda N, Makino N, Yamaguchi T, Yoshimura Y, Suematsu M. Leydig cell-derived heme oxygenase-1 regulates apoptosis of premeiotic germ cells in response to stress. J Clin Invest 2002;109:457-467.
4. Song R, Zhou Z, Kim PK, Shapiro RA, Liu F, Ferran C, et al. Carbon monoxide promotes Fas/CD95-induced apoptosis in Jurkat cells. J Biol Chem 2004;279:44327-44334.
5. Mori M, Suematsu M, Kyokane T, Sano T, Suzuki H, Yamaguchi T, et al. Carbon monoxide-mediated alterations in paracellular permeability and vesicular transport in acetaminophen-treated perfused rat liver. HEPATOLOGY 1999;30:160-168.
6. Kyokane T, Norimizu S, Taniai H, Yamaguchi T, Takeoka S, Tsuchida E, et al. Carbon monoxide from heme catabolism protects against hepatobiliary dysfunction in endotoxin-treated rat liver. Gastroenterology 2001;120:1227-1240.
7. Zhao Y, Brandish PE, Ballou DP, Marletta MA. A molecular basis for nitric oxide sensing by soluble guanylate cyclase. Proc Natl Acad Sci U S A 1999;96:14753-14758.
8. Otterbein LE, Bach FH, Alam J, Soares M, Tao Lu H, Wysk M, et al. Carbon monoxide has anti-inflammatory effects involving the mitogen-activated protein kinase pathway. Nat Med 2000;6:422-428.
9. Abraham NG, Quan S, Mieyal PA, Yang L, Burke-Wolin T, Mingone CJ, et al. Modulation of cGMP by human HO-1 retrovirus gene transfer in pulmonary microvessel endothelial cells. Am J Physiol Lung Cell Mol Physiol 2002;283:L1117-L1124.
10. Hill M, Pereira V, Chauveau C, Zagani R, Remy S, Tesson L, et al. Heme oxygenase-1 inhibits rat and human breast cancer cell proliferation: mutual cross inhibition with indoleamine 2,3-dioxygenase. FASEB J 2005;19:1957-1968.
11. Thomas SR, Mohr D, Stocker R. Nitric oxide inhibits indoleamine 2,3-dioxygenase activity in interferon-gamma primed mononuclear phagocytes. J Biol Chem 1994;269:14457-14464.
12. Shinoda Y, Suematsu M, Wakabayashi Y, Suzuki T, Goda N, Saito S, et al. Carbon monoxide as a regulator of bile canalicular contractility in cultured rat hepatocytes. HEPATOLOGY 1998;28:286-295.
13. Wakabayashi Y, Takamiya R, Mizuki A, Kyokane T, Goda N, Yamaguchi T, et al. Carbon monoxide overproduced by heme oxygenase-1 causes a reduction of vascular resistance in perfused rat liver. Am J Physiol 1999;277:G1088-G1096.
14. Fujii K, Sakuragawa T, Kashiba M, Sugiura Y, Kondo M, Maruyama K, et al. Hydrogen sulfide as an endogenous modulator of biliary bicarbonate excretion in the rat liver. Antioxid Redox Signal 2005;7:788-794.
15. Vreman HJ, Wong RJ, Kadotani T, Stevenson DK. Determination of carbon monoxide (CO) in rodent tissue: effect of heme administration and environmental CO exposure. Anal Biochem 2005;341:280-289.

16. Motterlini R, Clark JE, Foresti R, Sarathchandra P, Mann BE, Green CJ. Carbon monoxide-releasing molecules: characterization of biochemical and vascular activities. Circ Res 2002;90:e17-e24.
17. Bossard R, Stieger B, O'Neill B, Fricker G, Meier PJ. Ethinylestradiol treatment induces multiple canalicular membrane transport alterations in rat liver. J Clin Invest 1993;91:2714-2720.
18. Soga T, Baran R, Suematsu M, Ueno Y, Ikeda S, Sakurakawa T, et al. Differential metabolomics reveals ophthalmic acid as an oxidative stress biomarker indicating hepatic glutathione consumption. J Biol Chem 2006;281:16768-16776.
19. Kinoshita A, Tsukada K, Soga T, Hishiki T, Ueno Y, Nakayama Y, et al. Roles of hemoglobin allostery in hypoxia-induced metabolic alterations in erythrocytes: simulation and its verification by metabolome analysis. J Biol Chem 2007;282:10731-10741.
20. Goda N, Suzuki K, Naito M, Takeoka S, Tsuchida E, Ishimura Y, et al. Distribution of heme oxygenase isoforms in rat liver: topographic basis for carbon monoxide-mediated microvascular relaxation. J Clin Invest 1998; 101:604-612.
21. Yonetani T, Tsuneshige A, Zhou Y, Chen X. Electron paramagnetic resonance and oxygen binding studies of alpha-nitrosyl hemoglobin: a novel oxygen carrier having NO-assisted allosteric functions. J Biol Chem 1998; 273:20323-20333.
22. Suganuma K, Tsukada K, Kashiba M, Tsuneshige A, Furukawa T, Kubota T, et al. Erythrocytes with T-state-stabilized hemoglobin as a therapeutic tool for postischemic liver dysfunction. Antioxid Redox Signal 2006;8: 1847-1855.
23. Meier M, Janosik M, Kery V, Kraus JP, Burkhard P. Structure of human cystathionine beta-synthase: a unique pyridoxal 5'-phosphate-dependent heme protein. EMBO J 2001;20:3910-3916.
24. Taoka S, Banerjee R. Characterization of NO binding to human cystathionine beta-synthase: possible implications of the effects of CO and NO binding to the human enzyme. J Inorg Biochem 2001;87:245-251.
25. Prudova A, Bauman Z, Braun A, Vitvitsky V, Lu SC, Banerjee R. S-adenosylmethionine stabilizes cystathionine beta-synthase and modulates redox capacity. Proc Natl Acad Sci USA 2006;103:6489-6494.
26. Zhao W, Zhang J, Lu Y, Wang R. The vasorelaxant effect of H_2S as a novel endogenous gaseous K_{ATP} channel opener. EMBO J 2001;20:6008-6016.
27. Werstuck GH, Lentz SR, Dayal S, Hossain GS, Sood SK, Shi YY, et al. Homocysteine-induced endoplasmic reticulum stress causes dysregulation of the cholesterol and triglyceride biosynthetic pathways. J Clin Invest 2001;107:1263-1273.
28. Maher JM, Dieter MZ, Aleksunes LM, Slitt AL, Guo G, Tanaka Y, et al. Oxidative and electrophilic stress induces multidrug resistance-associated protein transporters via the nuclear factor-E2-related factor-2 transcriptional pathway. HEPATOLOGY 2007;46:1597-1610.
29. Sasaki H, Sato H, Kuriyama-Matsumura K, Sato K, Maebara K, Wang H, et al. Electrophile response element-mediated induction of the cystine/glutamate exchange transporter gene expression. J Biol Chem 2002;277: 44765-44771.
30. Fiorucci S, Antonelli E, Mencarelli A, Orlandi S, Renga B, Rizzo G, et al. The third gas: H_2S regulates perfusion pressure in both the isolated and perfused normal rat liver and in cirrhosis. HEPATOLOGY 2005;42:539-548.
31. Suematsu M, Ishimura Y. The heme oxygenase-carbon monoxide system: a regulator of hepatobiliary function. HEPATOLOGY 2000;31:3-6.
32. Kato Y, Shimazu M, Kondo M, Uchida K, Kumamoto Y, Wakabayashi G, et al. Bilirubin rinse: a simple protectant against the rat liver graft injury mimicking heme oxygenase-1 preconditioning. HEPATOLOGY 2003;38:364-373.
33. Sano T, Shiomi M, Wakabayashi Y, Shinoda Y, Goda N, Yamaguchi T, et al. Endogenous carbon monoxide suppression stimulates bile acid-dependent biliary transport in perfused rat liver. Am J Physiol 1997;272:G1268-G1275.
34. Norimizu S, Kudo A, Kajimura M, Ishikawa K, Taniai H, Yamaguchi T, et al. Carbon monoxide stimulates mrp2-dependent excretion of bilirubin-IXα into bile in the perfused rat liver. Antioxid Redox Signal 2003;5:449-456.
35. Nathanson MH, Burgstahler AD, Mennone A, Dranoff JA, Rios-Velez L. Stimulation of bile duct epithelial secretion by glybenclamide in normal and cholestatic rat liver. J Clin Invest 1998;101:2665-2676.
36. Spirli C, Fiorotto R, Song L, Santos-Sacchi J, Okolicsanyi L, Masier S, et al. Glibenclamide stimulates fluid secretion in rodent cholangiocytes through a cystic fibrosis transmembrane conductance regulator-independent mechanism. Gastroenterology 2005;129:220-233.
37. Sellers ZM, Mann E, Smith A, Ko KH, Giannella R, Cohen MB, et al. Heat-stable enterotoxin of Escherichia coli (STa) can stimulate duodenal HCO_3^- secretion via a novel GC-C- and CFTR-independent pathway. FASEB J 2008;22:1306-1316.
38. Boon EM, Huang SH, Marletta MA. A molecular basis for NO selectivity in soluble guanylate cyclase. Nat Chem Biol 2005;1:53-59.
39. Kajimura M, Shimoyama M, Tsuyama S, Suzuki T, Kozaki S, Takenaka S, et al. Visualization of gaseous monoxide reception by soluble guanylate cyclase in the rat retina. FASEB J 2003;17:506-508.
40. Imai T, Morita T, Shindo T, Nagai R, Yazaki Y, Kurihara H, et al. Vascular smooth muscle cell-directed overexpression of heme oxygenase-1 elevates blood pressure through attenuation of nitric oxide-induced vasodilation in mice. Circ Res 2001;89:55-62.
41. Ishikawa M, Kajimura M, Adachi T, Maruyama K, Makino N, Goda N, et al. Carbon monoxide from heme oxygenase-2 is a tonic regulator against NO-dependent vasodilatation in the adult rat cerebral microcirculation. Circ Res 2005;97:e104-e114.

Circ J 2009; **73:** 540–548

Important Regulatory Role of Activated Platelet-Derived Procoagulant Activity in the Propagation of Thrombi Formed Under Arterial Blood Flow Conditions

Noriko Tamura, MS; Isao Kitajima, MD**; Yota Kawamura, MD; Eri Toda, MD; Yu Eguchi, MD; Hideyuki Ishida, MD*; Shinya Goto, MD

Background: The functional links between the activation of platelets and the coagulation system have not been clarified.

Methods and Results: Immobilized collagen fibrils were perfused with human blood containing fluoresceinated platelets in the presence of various concentrations of thrombin inhibitor. Coagulant activity around platelet thrombi was detected using a FITC-conjugated antibody against the fibrin monomer complex (F-405). Intra-cytosolic calcium ion concentrations ($[Ca^{2+}]_i$) in individual platelets and the volume of thrombi were detected with an ultrafast confocal laser microscope equipped with a piezo-motor control unit. The volume of platelet thrombi formed after 8 min of blood perfusion in the presence of 10, 25, 50, and 100 μmol/L argatroban was 7.69±0.46 μm^3, 6.61±1.96 μm^3, 3.63±1.54 μm^3, and 1.67±0.75 μm^3, respectively. There was a positive correlation between the volume of platelet thrombi and the amount of fibrin monomer complex produced around them. The $[Ca^{2+}]_i$ of the platelets forming the thrombi oscillated between a minimum of 92.0±57.4 nmol/L, 120.1±68.1 nmol/L, and a maximum of 217.6±131.5 nmol/L, 367.6±189.1 nmol/L, respectively, in the presence of 100 and 10 μmol/L argatroban.

Conclusions: The results suggest a crucial role of coagulant activity in both the generation of fibrin and the growth of platelet thrombi. (*Circ J* 2009; **73:** 540–548)

Key Words: Blood flow; Calcium; Fibrin monomer complex; Platelet; Thrombin

Thrombi causing the "so-called atherothrombotic diseases"[1] contain at least 3 components: platelets, fibrin, and inflammatory cells[2,3] The functions and activation mechanisms of the platelets[4,5] the coagulation cascade[6,7] and the inflammatory cells[8] have been investigated extensively. Now, attention is being focused on the functional links among these components during the formation of thrombi large enough to cause symptomatic atherothrombosis[9,10–13]

Indeed, platelets adhere and accumulate at sites of endothelial damage and are known to play a central role in the local regulation of coagulation and inflammation (eg, platelets have a procoagulant membrane component on their surface upon activation[14,15] express adhesive molecules[16] to capture inflammatory cells in the thrombi, release inflammatory cytokines such as the CD40 ligand[17–19] and procoagulant microparticles[20,21]). Local activation of coagulation and inflammation that occurs around the activated platelets themselves may influence the functions of the platelets through stimulation of various receptors, such as protease-activated receptors (mostly PAR1, but also PAR4[22]);[23] ADP receptors;[14] integrins;[24] etc); however, these mechanisms are still not fully understood![1,11,12]

In the present study, we investigated the functional interrelationships between platelets and the coagulation system under arterial blood flow conditions, although the later is believed to be activated in vivo mostly at sites of blood stagnation.

Methods

Preparation of Blood Samples, Artificial Blood Flow Conditions, and Measurement of the $[Ca^{2+}]_i$ of Platelets Incorporated in Thrombi

Venous blood samples were collected from 10 adult volunteers after obtaining their written informed consent. The investigation conformed with the principles of the Declaration of Helsinki and the study protocol was approved by the Internal Review Board of Tokai University. All of the study subjects (8 men, 2 women; age 28–44 years) were instructed to abstain from drugs known to interfere with platelet function during the month preceding the study. The blood specimens were immediately transferred into plastic tubes containing 1/10 volume of the specific thrombin inhibitor argatroban (Mitsubishi Kagaku, Tokyo, Japan) at final concentrations ranging from 10 to 100 μmol/L, to test for antithrombin effects on the formation of fibrin around the

(Received May 16, 2008; revised manuscript received October 7, 2008; accepted October 19, 2008; released online January 29, 2009)

*Department of Medicine, *Department of Basic Science, Tokai University School of Medicine, Isehara and **Department of Clinical Laboratory and Molecular Pathology, University of Toyama, Toyama, Japan*

Mailing address: Shinya Goto, MD, Department of Medicine, Tokai University School of Medicine, 143 Shimokasuya, Isehara 259-1143, Japan. E-mail: sgoto3@mac.com

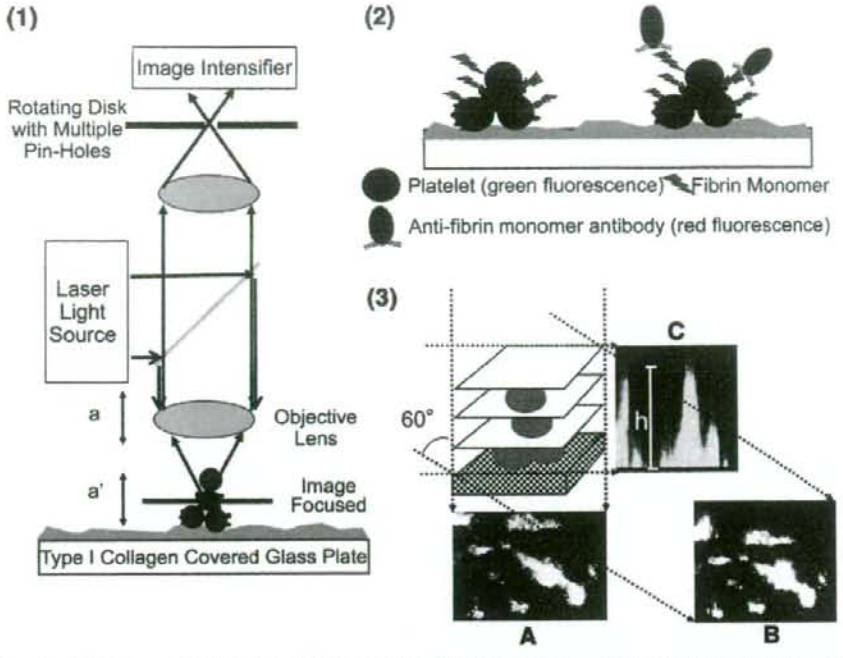

Figure 1. Multicolor and 3-dimensional (D) imaging of the thrombi formed under arterial blood flow conditions. Type I collagen fibrils were perfused with blood containing fluoresceinated platelets for 8 min at a wall shear rate of 1,500/s in a rectangular flow chamber. Thrombi formed on the collagen fibrils were visualized using both an epi-fluorescent multicolor video-microscope and the newly developed ultra-fast confocal laser microscope equipped with a piezo-motor control unit, as depicted schematically on the left-hand side. The activation of platelet-derived procoagulant activity was detected as the appearance of the fibrin monomer complex around the platelet thrombi visualized (in red), while platelets were visualized in green. The objective lens was moved up and down at a constant speed of 0.4 μm/s under the control of the piezo-motor control unit (a) to obtain scanning images of the platelet thrombi (a'). The sum of the scanning confocal images from the bottom to the top was projected on planes at 10-degree intervals relative to the x-axis to obtain the 3-D projection images shown on the right-hand side, including the projections at 0 degrees (top view, **A**), 60 degrees (**B**) and 90 degrees (front view, **C**). The maximum height (h) of the platelet thrombi was calculated from the frontal projection image, as shown in **C**.

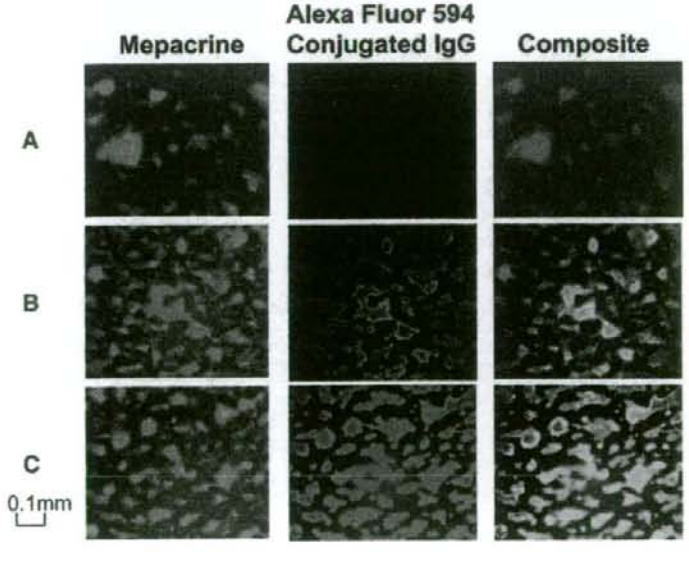

Figure 2. Specific detection of the fibrin monomer complex around the platelet thrombi. Platelet thrombi formed as a result of perfusion of the collagen fibrils with whole blood for 8 min (Left). Next, they were incubated with HEPES-NaCl solution (pH 7.4) containing either 1 of the monoclonal antibodies, negative control antibody against thyroglobulin (T_Y), human fibrin monomer complex (F-405), or positive control antibody against the platelet surface protein GPIbα (GUR20-5) at a concentration of 5 μg/ml for 15 min. The specificity of the red fluorescence staining in the presence of anti-human fibrin monomer complex antibody (**B**) was confirmed by comparison with the staining results obtained with negative (**A**) and positive (**C**) control antibody. Superimposition of the green and red fluorescence staining images revealed the prominent presence of the fibrin monomer complex on the surface of the platelet thrombi.

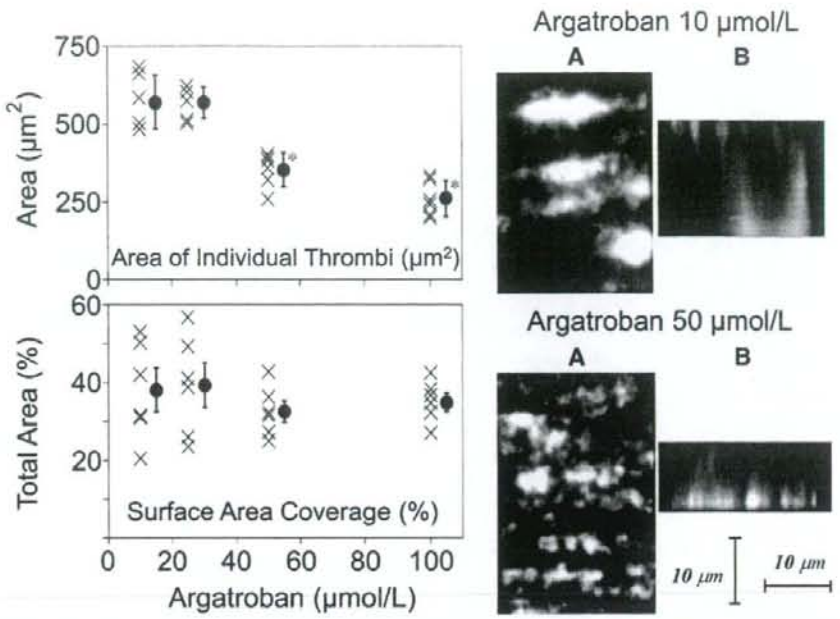

Figure 3. Relationship between inhibition of the function of thrombin and the 2- and 3-dimensional (D) growth of the platelet thrombi formed on the collagen fibrils by blood perfusion at a wall shear rate of 1,500/s. Immobilized collagen fibrils in the rectangular flow chamber were perfused with blood samples containing the specific thrombin inhibitor argatroban (10–100 μmol/L) at varying final concentrations for 8 min at a wall shear rate of 1,500/s. Projection images at (**A**) 0 degrees along the x-axis corresponding to the projection from the top of the thrombi and (**B**) 90 degrees along the x-axis corresponding to the projection from the side of the thrombi. Quantitative results obtained from these 3-D images are summarized in Table 1. Quantitative surface area coverage by individual platelet thrombi, (**Lower left**) total area covered by the platelets. The results demonstrate the mean and standard error of 6 different experiments. *Significantly smaller value than that obtained by 8 min of perfusion of blood containing the lowest concentration of antithrombin tested in the study (10 μmol/L).

Table 1. Surface Area Coverage, Height and Volume of Individual Thrombi Formed on the Collagen Fibrils After 8 min of Perfusion of Blood Containing Various Concentrations of Antithrombin

Argatroban (μmol/L)	10	25	50	100
Area (μm^2)	576.7±–81.3	555.0±181.4	359.1±111.1*	256.7±47.3*
Height (μm)	17.6±2.8	14.9±1.6	13.7±3.0*	10.4±0.6*
Volume (mm^3)	7.69±0.46	6.61±1.96	3.63±1.54*	1.67±0.75*

*Value is significantly smaller than that obtained after 8 min of perfusion of blood containing the lowest concentration of argatroban used in the study (10 μmol/L). The same value is significantly smaller than that obtained in the presence of 25 or 50 μmol/L of argatroban.

platelet thrombi, on calcium signaling, and on the growth of the platelet thrombi[25–27] Clinically relevant anticoagulants, including unfractionated heparin and low-molecular-weight heparin, were also tested, but the results could not be included because the blood coagulated during experiments.

For the experiments conducted to examine the growth of the thrombi and imaging of the platelet-derived procoagulant activity, platelets in whole blood samples were rendered fluorescent by the addition of mepacrine (Sigma Chemical Co, St Louis, MO, USA)[25,27,28] For the experiments conducted to measure the intra-cytosolic calcium ion concentrations ($[Ca^{2+}]_i$), the platelets were loaded with the calcium-sensitive dye, fluo-3AM, in accordance with a previously described procedure[29] with slight modification[26] Fluo-3 loaded platelets were re-suspended in homologous, initially separated platelet-poor plasma containing the antithrombin agent argatroban at a concentration of 10 or 100 μmol/L. The hematocrit of the final cell suspension was adjusted to 40%.

A rectangular flow chamber with its glass bottom coated with immobilized type I collagen fibrils was assembled as described previously[14,25,28] The experimental blood samples were aspirated into the chamber with a syringe pump (Harvard Apparatus, Holliston, MA, USA) for 8 min at a constant flow rate to obtain a wall shear rate of 1,500/s unless otherwise specified (limited number of experiments were conducted at shear rate 0 and 100/s).

Imaging of the Platelet Thrombi and Measurement of Platelet-Derived Procoagulant Activity

The platelet thrombi were initially visualized using an inverted-stage epi-fluorescence video-microscopy system connected to a 480-nm excitation light source (DM IRB, 1RB-FLUO, Leica, Germany)[14,25] To quantify the 2-dimensional (D) growth of the platelet thrombi, both the surface

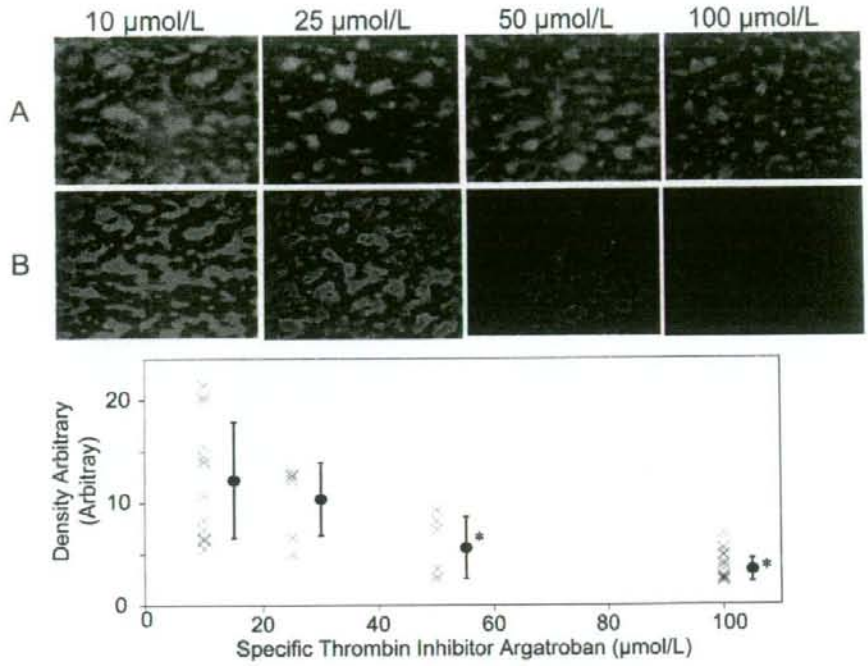

Figure 4. Relationship between functional inhibition of thrombin and the generation of the fibrin monomer complex around the platelet thrombi. The experiments were conducted in a similar manner as described in Figure 3. Dual-color fluorescence imaging was performed after washing with secondary antibody 3 times with 5 ml of HEPES-NaCl solution (pH 7.4). Fluoresceinated platelets (green), and fibrin monomers (red) were visualized using a barrier filter centered at the wavelengths of 527 nm (**A**) and 600 nm (**B**), respectively. Quantitative densitometry was performed to detect the total amount of fibrin monomers formed around the platelet thrombi, and the results are summarized in the lower panel.

area coverage of individual platelet thrombi (μm^2) and the total surface area coverage of the platelets (%) were calculated[25] The 3-D projection images of the platelet thrombi were also obtained with a fast confocal laser microscope equipped with a piezo-motor control unit, as described previously[26,30,31] (**Figure 1**). The 3-D projection images of the thrombi were obtained using the ImageJ 1.29v program (National Institutes of Health, Bethesda, MD, USA), as shown in **Figure 1**[26,30,31] The maximum height of the thrombi was calculated from a 90-degree (front) projection image, and the volume of each thrombus was derived by integration of the cumulative cross-sectional area occupied by the platelets in confocal sections obtained at 0.2-μm intervals.

For imaging of the activation of the coagulation cascade on the surface of the platelet thrombi (platelet-derived procoagulant activity), HEPES-NaCl solution (pH 7.4) containing mouse-derived monoclonal antibody against the human fibrin monomer complex F-405[32] at a final concentration of 5 μg/ml was incubated with the platelet thrombi formed after 8 min of blood perfusion (**Figure 1**). The presence of the anti-fibrin monomer complex antibody on the platelet thrombi was detected using Alexafluor594-conjugated goat-derived anti-mouse polyclonal IgG (Molecular Probes, Inc, OR, USA) at a final concentration of 10 μg/ml. Both FITC-conjugated Annexin V (kindly provided by Dr Nomura, Kansai University, Osaka, Japan) and Alexafluor594-conjugated monoclonal antibody against tissue factor ATN-8 (kindly provided by Chugai, Co Ltd, Gotenba, Japan) were used in some experiments to detect the distribution of negatively charged phospholipids and/or tissue factor on and/or around the platelet thrombi[15,33] Dual-color fluorescence imaging, to detect platelets as green and the fibrin monomer complex as red, was performed after the washing procedure with a barrier filter centered at wavelengths of 527 nm and 600 nm, respectively (**Figure 2**). The specificity of detection of the fibrin monomer complex by this method was confirmed by comparison with the same concentration of iso-type matched negative and positive control IgG (GUR20-5: antibody against platelet GPIbα, kindly provided by Dr Handa, Keio University, Tokyo, Japan) as shown in **Figure 2**. Quantitative densitometry was performed to measure the total amount of fibrin monomer complex formed around the platelet thrombi using the same method as that described previously to estimate the amount of platelet accumulation[27]

Real-Time Imaging to Measure $[Ca^{2+}]_i$ in Platelets Forming Thrombi Under Blood Flow Conditions

The $[Ca^{2+}]_i$ of the platelets forming thrombi was measured using the same confocal microscopy system described previously[29,26] but without the use of the piezo-motor control unit. Variations in the fluorescence intensity of the fluo-3AM-loaded platelets were converted into $[Ca^{2+}]_i$ using the equation:

$$[Ca^{2+}]_i = Kd(F - Fmin)/(Fmax - F),$$

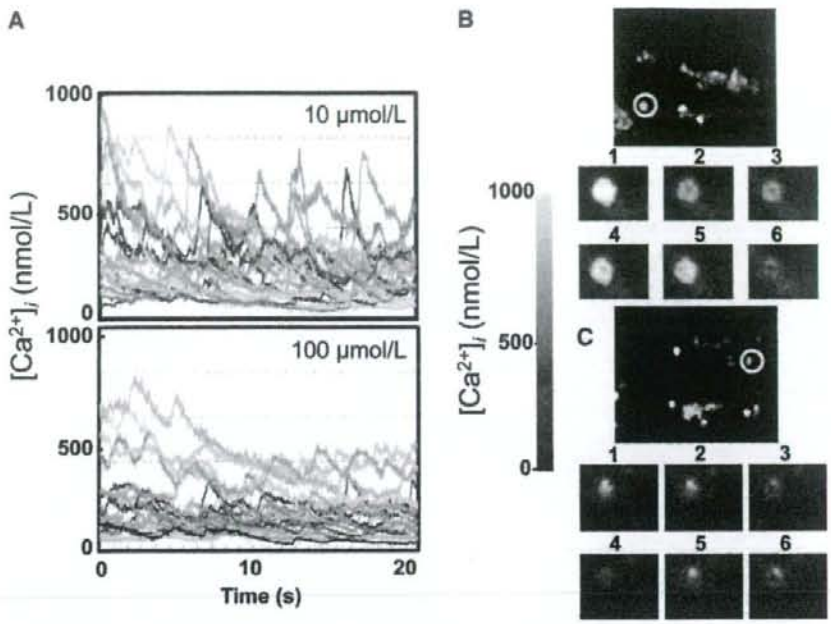

Figure 5. Changes in the $[Ca^{2+}]_i$ of the platelets forming the thrombi on the collagen fibrils under blood flow conditions. These experiments were conducted as described in Figure 3, except that the blood was replaced with a cell suspension containing fluo-3AM-loaded platelets, washed erythrocytes and homologous platelet-poor plasma with the specific thrombin inhibitor argatroban at 2 different concentrations, 10 and 100 μmol/L. (**Left: A**) $[Ca^{2+}]_i$ of 10 randomly selected platelets recorded over a 10-s period beginning 2 min after the start of the blood perfusion, (**Right**) fluorescence images reflecting the $[Ca^{2+}]_i$ in individual platelets starting to adhere to the collagen surface in the presence of 10 μmol/L (**B**) and 100 μmol/L (**C**) of specific thrombin inhibitor argatroban. The results shown are representative of 4 different experiments.

where Kd is the dissociation constant of fluo-3AM in the interaction with Ca^{2+} (corresponding to 495 nmol/L at 25°C)[34] F is the measured fluorescence intensity of a single platelet, Fmax is the fluorescence intensity of a single platelet treated with the Ca^{2+} ionophore A23187 (10 μmol/L; Sigma) in the presence of 2 mmol/L calcium chloride, and Fmin is the fluorescence intensity of an unstimulated single platelet. To examine whether the changes in the $[Ca^{2+}]_i$ were related to trans-membrane entry or changes in the intracellular distribution, the effects of lanthanum chloride, a putative calcium-channel blocker, were tested[26,35]

Statistical Analysis

All numerical data are expressed as mean ± SD, unless otherwise specified. The effect of various concentrations of argatroban on the growth of the platelet thrombi was tested by 1-way analysis of variance (ANOVA). Differences between 2 groups of data were evaluated by Newman-Keuls test; $P<0.05$ was considered to denote statistical significance.

Results

Inter-Relationship Between Inhibition of the Coagulation Cascade and Growth of Platelet Thrombi

As shown in **Figure 3**, the size of the individual thrombi that formed on the collagen fibrils was smaller after perfusion of blood containing higher concentrations of thrombin inhibitor. Quantitative analysis revealed that the area covered by individual platelet thrombi in the presence of thrombin inhibitor at concentrations of 50 and 100 μmol/L was significantly smaller than that formed in the presence of 10 μmol/L ($P<0.05$), as shown in **Figure 3** and **Table 1**. The total surface area covered by the platelets was not significantly influenced by the concentration of thrombin inhibitor, indicating that a larger number of smaller thrombi formed in the presence of higher concentrations of thrombin inhibitor.

The 3-D projection imaging of the platelet thrombi using our newly developed confocal imaging technique revealed that the height and volume of individual thrombi formed after 8 min of perfusion of blood containing lower concentrations of thrombin inhibitor were larger than those formed after perfusion of blood containing higher concentrations of the same inhibitor (**Figure 3, Table 1**).

Activation of the Coagulant Cascade Around Activated Platelets and the Role in Maintaining the Activated State of Platelets Incorporated Into Thrombi Under Arterial Blood Flow Conditions

As shown in the upper panels of **Figure 4**, there was a larger amount of fibrin monomer complex, detected as red fluorescence, around the platelet thrombi formed in the presence of lower concentrations of thrombin inhibitor. A similar distribution of FITC-conjugated Annexin V could be detected under the same conditions, whereas neither tissue factor nor tissue-factor-bearing microparticles, a homogeneous distribution of which could be detected by our imaging system, were detected around the platelet thrombi (data not shown). Quantitative densitometric analysis, shown

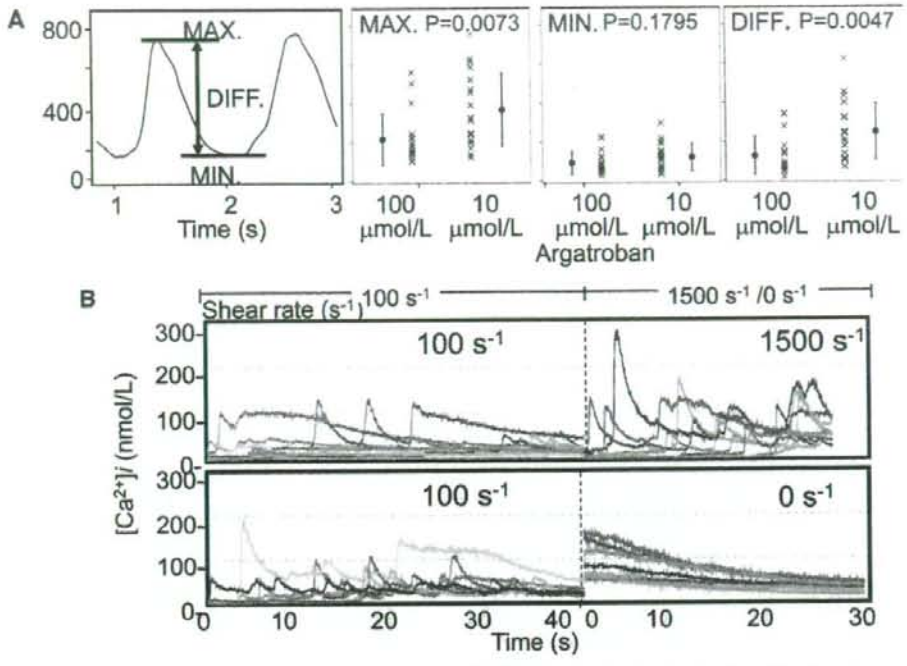

Figure 6. Quantitative results of $[Ca^{2+}]_i$ and changes in the $[Ca^{2+}]_i$ of the platelets forming the thrombi on the collagen fibrils under various shear rates. (**A**) These experiments were conducted as described in Figure 6. The minimum (MIN.), maximum (MAX.) and difference (DIFF.) between the minimum and maximum $[Ca^{2+}]_i$ defined in the upper right panel were calculated for 20 randomly selected platelets in 4 different experiments. The mean values and the SD are shown. (**B**) These experiments were conducted as described in Figure 6, except that the shear rate was changed as shown in the upper panel. Each line represents the $[Ca^{2+}]_i$ in individual platelets under shear rates shown above. Results shown are the 4 different experiments in the presence of 100 μmol/L of specific thrombin inhibitor argatroban.

in the lower panel of **Figure 4**, demonstrates the dose-dependent inhibitory effects of thrombin inhibitor on the generation of the fibrin monomer complex around the platelet thrombi formed under arterial blood flow conditions.

The $[Ca^{2+}]_i$ of the platelets adhering to the collagen fibrils is shown in **Figure 5A**. A cyclic increase in the $[Ca^{2+}]_i$ occurred in the majority of individual platelets adhering to the immobilized collagen fibrils, although the strength and cycle length of the oscillations were not homogeneous. The addition of the putative calcium-channel blocker, lanthanum chloride, at a final concentration of 1 mmol/L to the blood samples completely blocked these cyclic increases in the $[Ca^{2+}]_i$[26] (data not shown). There was, however, a tendency for the maximum increase in the $[Ca^{2+}]_i$ to be greater in the presence of lower concentrations of thrombin inhibitor. Indeed, quantitative analysis of 20 randomly selected platelets in 4 different experiments revealed that both the maximum value and the differences between the maximum and minimum values of $[Ca^{2+}]_i$ were significantly higher in the presence of 10 μmol/L argatroban than the corresponding values in the presence of 100 μmol/L of the same inhibitor (**Figure 6A**). We also demonstrated that the cyclic increase in the $[Ca^{2+}]_i$ is shear rate dependent and disappears at a shear rate of 0 (**Figure 6B**).

Discussion

In the present study, we demonstrated activation of the coagulation cascade around platelet thrombi formed under arterial blood flow conditions, as evidenced by the appearance of fibrin monomer complexes around the platelet thrombi. We have also demonstrated that the cyclic increase in $[Ca^{2+}]_i$ in each platelet incorporated into the thrombi, which is assumed to represent the sum of the activation signals of the platelet and has been shown to be influenced by shear rate and the presence of specific thrombin inhibitor, positively correlates with the 3-D growth, especially in the z-section, of the platelet thrombi. Our experimental results suggest an important regulatory role of thrombin generated on the surface of activated platelets as a result of the procoagulant activity in both the formation of fibrin around the platelets and the maintenance of the activated state of platelets incorporated into thrombi so that the platelet thrombi remain stable and, at least in our experimental conditions, the calcium-sensitive phospholipid scramblase[36,37] is activated to continue further expression of procoagulant phospholipid on the platelet thrombi (**Figure 7**)[38,39]

Our experimental results with human blood samples were in complete agreement with in vivo animal experiments published previously[33] Our findings fundamentally serve to confirm those animal experimental results, except that we used human blood in an in vitro setup without blood vessels. Obviously, our model does not pose any problems related to species differences, which is important in understanding the regulatory role of the activation of the coagulant cascade in the 3-D growth of platelet thrombi, because it is well

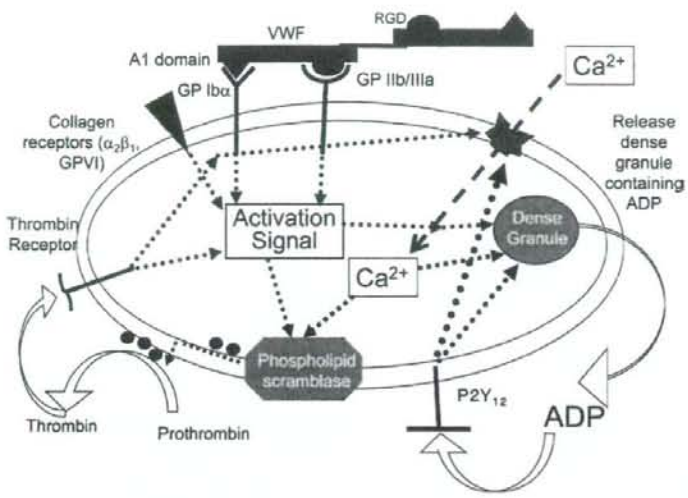

Figure 7. Regulatory role of platelet-derived procoagulant activity on the continuous activation of platelet and thrombus growth. Platelets, once they interact with subendothelial matrix such as collagen or von Willebrand factor (VWF)[48,49] activated to release ADP-containing dense granules. Next, the released ADP stimulates ADP receptors ($P2Y_1$ and $P2Y_{12}$). As previously demonstrated, continuous stimulation of $P2Y_{12}$ results in a cyclic increase in $[Ca^{2+}]_i$, which activates many Ca^{2+}-dependent enzymes, such as phospholipid scramblase. Activation of that enzyme increased the expression of procoagulant negatively charged phospholipid, which supports conversion of prothrombin to thrombin on the surface of the activated platelet. Thrombin generated on the surface of activated platelets further activates the platelet through thrombin receptors.

known that the thrombin receptor, a major possible regulator in humans, is a different moiety in mice. Indeed, protease-activated receptor,[40] which is the most important functional receptor of thrombin in humans, is not expressed on mouse platelets.[23] Perhaps the main limitations of our blood perfusion model, however, are the differences in the blood flow conditions and the matrix exposed to the blood stream we used from an in vivo setting. Moreover, we had to use at least a minimal amount of anticoagulant to maintain blood fluidity during our experiments, which could influence the generation and function of thrombin. Our experiments cannot assess the clinically relevant, low dose of anticoagulant (not only argatroban, but also unfractionated heparin, low-molecular-weight heparin, etc). Moreover, our method is not applicable for assessing the effects of various antiplatelet agents on platelet-derived procoagulant activity because it requires the formation of large-enough platelet thrombi on collagen fibrils, which is inhibited by antiplatelet agents. Our methodology to detect fibrin monomer is not sensitive enough to detect small changes at various shear rates. We are attempting overcome this limitation by improving imaging tool, but could not provide relevant results in the current report.

Despite these limitations, the thrombi that formed on the collagen fibrils in our experimental model, and comprised both activated platelets and fibrin, were basically the same as the pathological arterial thrombi causing myocardial infarction, although the latter contain a larger amount of insoluble fibrin fibrils.[2,3] Nevertheless, we believe that our main findings give new insights into the key role of activated platelet-derived procoagulant activity in the growth of thrombi. We propose this begins with activation of the platelets accumulating at a site of endothelial injury under blood flow conditions, followed by the appearance of activated-platelet-derived procoagulant activity[41] and the generation of thrombi on the membrane surface of activated platelets, even under arterial flow conditions, which results in both local fibrin fibril formation and in continuous activation of the platelets forming thrombi by repetitive stimulation of thrombin receptors, causing an increase in $[Ca^{2+}]_i$ to activate phospholipid scramblase[37] and further enhancing platelet-derived procoagulant activity,[42] as well as maintaining the stability of platelet thrombi for the development of large arterial occlusive thrombi (**Figure 7**).[26] There is an interesting previous publication showing that mice that are deficient in phospholipid scramblase do not express bleeding problems.[36] In this context, regulation of phospholipid scramblase might be a possible target of antiplatelet agents with least bleeding complications. Further investigation is awaited.

Nonetheless, our experimental results provide little information regarding the mechanism of induction of the platelet-derived procoagulant activity, the details of which are still to be clarified.[43,44] Previous reports have demonstrated the importance of the surface expression of negatively charged phospholipids, mostly phosphatidylserine,[45] which can be detected by Annexin V binding,[15] and its appearance was confirmed in our study in association with activation of the coagulation cascade on the surface of the activated platelets. It is also known that increased $[Ca^{2+}]_i$, which was shown in our study, especially in the presence of low concentrations of thrombin inhibitor (**Figure 6**), plays certain important roles in the activation of phospholipid scramblase,[26] resulting in surface exposure of phosphatidylserine.[46] Accordingly, our results showing an increase in the $[Ca^{2+}]_i$ of the platelet forming thrombi not only indicate the activated state of the platelets, but also the induction of procoagulant activity resulting in the appearance of the fibrin monomer complex. Indeed, a previous report demonstrated that factor IXa binding to platelet and generation of activated factor Xa was prevented by the putative Ca^{2+} channel-blocker of lanthanum chloride.[47] Unlike in vivo animal experiments[33,48] or atherothrombosis in humans,[2,3,6] our experiments did not include tissue factor originating from the vascular wall or ruptured atheroma. Thus, tissue factor, if it played a role in the generation of fibrin in our experiments, is limited to a blood-borne one.[48] The limitation to our experiments that a small amount of anticoagulant is required makes it impossible to assess whether the lower amount of fibrin fibril formation we observed is because of a lack of vessel-related tissue factor or represents the effects of antithrombin. The fact that we could detect neither soluble tissue factor nor accumulation of tissue-factor-bearing microparticles around the platelet thrombi in our experiments, despite the significant amount of tissue factor detected on the surface of the monocytes